



HAL
open science

Practical insights on standardised models for estimation of crack width due to imposed strains in edge-restrained reinforced concrete elements

Agnieszka Jędrzejewska, Mariusz Zych, Jean Michel Torrenti, Fragkoulis Kanavaris, Miguel Azenha, Fangjie Chen, Shintaro Ito

► To cite this version:

Agnieszka Jędrzejewska, Mariusz Zych, Jean Michel Torrenti, Fragkoulis Kanavaris, Miguel Azenha, et al.. Practical insights on standardised models for estimation of crack width due to imposed strains in edge-restrained reinforced concrete elements. *Engineering Structures*, 2024, 305, pp.117757. 10.1016/j.engstruct.2024.117757 . hal-04493430

HAL Id: hal-04493430

<https://hal.science/hal-04493430>

Submitted on 13 Mar 2024

HAL is a multi-disciplinary open access archive for the deposit and dissemination of scientific research documents, whether they are published or not. The documents may come from teaching and research institutions in France or abroad, or from public or private research centers.

L'archive ouverte pluridisciplinaire **HAL**, est destinée au dépôt et à la diffusion de documents scientifiques de niveau recherche, publiés ou non, émanant des établissements d'enseignement et de recherche français ou étrangers, des laboratoires publics ou privés.

1 Practical insights on standardised models for estimation of crack width due 2 to imposed strains in edge-restrained reinforced concrete elements

3 Agnieszka Jędrzejewska^{a,*}; Mariusz Zych^b; Jean Michel Torrenti^c; Fragkoulis Kanavaris^d; Miguel
4 Azenha^e; Fangjie Chen^f; Shintaro Ito^g

5 ^a Silesian University of Technology, Department of Structural Engineering, Akademicka 5, 44-100 Gliwice,
6 Poland

7 agnieszka.jedrzejewska@polsl.pl

8 ^b Cracow University of Technology, Reinforced Concrete Structures Division, Warszawska 24, 31-155
9 Kraków, Poland

10 mzych@pk.edu.pl

11 ^c Université Gustave Eiffel, Department of Materials and Structures, 16 Bd Newton, 77420 Champs-sur-
12 Marne, France

13 jean-michel.torrenti@univ-eiffel.fr

14 ^d ARUP, 8-13 Fitzroy St, London W1T 4BQ, UK

15 frag.kanavaris@arup.com

16 ^e University of Minho, ISISE, ARISE, Department of Civil Engineering, 4800-058 Guimarães, Portugal

17 miguel.azenha@civil.uminho.pt

18 ^f ARUP, Sky Park, 1 Melbourne Quarter, 699 Collins St, Docklands VIC 3008, Australia

19 sam.chen@arup.com

20 ^g ARUP, 8F Iidabashi Grand Bloom, 2-10-2 Fujimi Chiyoda-ku, Tokyo 102-0071, Japan

21 shintaro.ito@arup.com

22 * corresponding author; contact address: Agnieszka.Jedrzejewska@polsl.pl

23
24 **Abstract.** The paper presents a critical study on the predictive capacity of standardised methods for
25 crack width calculations in edge-restrained reinforced concrete elements subjected to imposed strains.
26 The aim of the presented integrative analysis was to reach global understanding of the issue of restraint-
27 induced cracking from the point of view of SLS design and to build a sound basis for future
28 developments of new models. The study covered relevant methods from Europe, Australia, Japan and
29 the USA. The study was performed on three distinct case studies: (i) a demonstration example; (ii) a
30 massive containment wall; and (iii) a heavily-reinforced tank wall segment. It was concluded that a
31 model for crack width control in edge-restrained elements should consider the stage of cracking and be
32 generalised for possible geometries and reinforcement. Agreement must be made on the properties of
33 concrete applied in the design, including effective tensile strength, effective modulus of elasticity (to
34 account for creep) and the level of strain relieve after crack formation with its effect on the crack width.

35 **Keywords:** crack control; standards; imposed strains; crack width; wall-on-slab; restraint.

36 **1 Introduction**

37 The aim of the serviceability limit state (SLS) design of cracking of reinforced concrete structures is
38 predominately to ensure durability of the structure but also to ensure its functionality. Crack width
39 control is especially important in structures with increased tightness requirements: water tightness or
40 restricted permeability [1]. These include structures in direct contact with ground water, such as
41 retaining walls, tunnels and bridge abutments, as well as tanks and various types of nuclear
42 containments. In addition to external mechanical loading acting during operation, these structures are
43 also subjected to the action of imposed strains. These imposed strains result from the effect of
44 temperature changes, shrinkage and creep, and may occur over the whole life of the structure, both at
45 the construction stage (autogenous shrinkage and temperature variation resulting from cement hydration
46 during hardening of concrete) and during operation (drying shrinkage and temperature variations
47 resulting from ambient temperature or service conditions) [2].

48 The design for restraint-induced cracking in reinforced concrete structures is a challenging endeavour.
49 It consists in general of three tasks: (i) quantification of imposed strains, (ii) assessment of the
50 restraining conditions, and (iii) determination of the required reinforcement for crack width control. In
51 design guidelines, the restraint is usually differentiated into **internal** and **external** restraint. In case of
52 the latter, a distinction should be made into (i) **end restraint**, where an element is externally restrained
53 at its extremities, (ii) **edge restraint**, where an element is externally restrained along its edge, usually
54 the base, and (iii) **combined restraint** where an element is restrained along multiple edges. This paper
55 focuses on the SLS design of the edge-restrained elements which represent a range of the wall structures,
56 majority of which are the structures with the increased tightness requirements.

57 Even though there exist design methods throughout the engineering community (some of which have
58 been implemented into design guidelines and standards), there is no agreement on the formulation for
59 the crack width calculation in reinforced concrete elements subjected to the restraint-induced cracking.

60 A systematic overview was needed of the available methods. So far, such state-of-the-art studies have
61 been done for crack width estimation methods in flexural elements, see e.g. the works of *Borosnyői and*
62 *Balazs* [3] or more recent work of *Lapi et al.* [4]. Chosen standardised methods for crack width

63 calculations in wall structures (EN 1992-1-1:2004 [5] & EN 1992-3:2006 [6], CIRIA C660 [7], ACI
64 207.2 [8] and JCI Guideline [9]) have been comparatively studied by *Klemczak and Žmij* [10]. A review
65 on the crack width estimations in edge-restrained elements according to these guidelines has been also
66 done by *Zych* [11] in addition to the analysis of various non-standardised analytical models. Finally, an
67 extensive review of the standardised methods for the restraint-induced cracking of reinforced concrete
68 structures has been presented by the authors in [12]. The comparative study covered all relevant design
69 methods implemented in the guidelines worldwide, and included European standards: EN 1992-1-
70 1:2004 [5], EN 1992-3:2006 [6] and the latest available at the time version of the final draft FprEN
71 1992-1-1 [13] (now issued with minor changes as an official version EN 1992-1-1:2023 [14]), as well
72 as British guideline CIRIA C766 [15]; Australian recommendations CIA Z7/06 [16]; Japanese
73 recommendations AIJ-SRC **Erreur ! Source du renvoi introuvable.**, and American ACI reports
74 207.2R-07 [8] and 224R-01 [18], and covered both end-restrained and edge-restrained elements.
75 The overview of the design methods showed that the main difference between the methods lays in the
76 assumptions of the model. There exist proposals based purely on the empirical or experimental bases,
77 and these have not been implemented for design [11]. The current version of the JCI Guideline is, in
78 turn, fully based on the extensive FEM-based calculations and thus has no direct physical meaning, as
79 explained by the authors in [12]. Regarding the standardised methods, majority of the currently used
80 guidelines, namely those following the philosophy of EN 1992-1-1:2004 [5], assume the same bond
81 strength for the crack formation stage and stabilised cracking stage, which results in the same value of
82 the transfer length in both cracking stages, although for the crack formation stage the calculated $s_{r,max}$
83 should be interpreted as twice the transfer length ($s_{r,max} = 2l_{e,max}$) while for the stabilised cracking as
84 the crack spacing. The same models for crack spacing as for the elements in direct tension are
85 recommended for the design of the elements subjected to the restraint of imposed strains. Only some of
86 the design guidelines explicitly acknowledge the fact that the cracking caused by the restraint of
87 imposed strains is governed by the single-crack condition (crack formation phase). These include AIJ-
88 SRC [17] and the design method implemented in the ACI 207.2-95 [19], which is no longer a valid
89 standard. The differences in the methods result also from the way in which the values of relevant input

90 parameters are determined in the method. This relates to the magnitude of the imposed strains, effective
91 tensile strength, reinforcement ratio, effect of creep and degree of restraint.

92 Consequently, experience of the authors has shown that crack width estimates may vary significantly
93 depending on which model is used, however, no systematic studies comparing the predictive capacities
94 of the methods have been identified in the literature. In general, the comparative studies are usually
95 limited to a given group of models based on the same philosophy where calibrations are proposed to
96 modify the models to obtain better compliance between the experimental measurements and calculation
97 results. Among numerous studies, one can mention the works comparing the past version of EN 1992-
98 3:2006 and CIRIA C766 in their predictive capacity to evaluate the expected crack widths in edge-
99 restrained walls, such as the study of *El Khoury et al.* [20] on laboratory tests of mock-up walls or the
100 study of *Jędrzejewska et al.* [1] on the experiences from in-situ cracking of wall-on-slab structures.

101 Both works indicated significant discrepancies of both approaches regarding the compliance of the
102 measurements and calculations. Analogous comparisons have been made between the previous and new
103 version of EN 1992 as well as between FprEN 1992-1-1 and CIRIA C766 by e.g. *Klausen* [21], as the
104 main aim of the new guidelines of Eurocode 2 has been to improve the predictive capacity of the model
105 initially proposed in EN 1992-1-1:2004 & EN 1992-3:2006. Nevertheless, the performance of the EN
106 1992-1-1:2023 [14] model on real-scale wall-type structures has not yet been investigated. Here, one
107 should also mention the extensive study performed by CROW-CUR in the Netherlands where a
108 modification to the EN 1992-1-1:2004 [5] formula for crack spacing has been proposed based on the
109 analysis of cracking observed in-situ on a large set of real-life structures. In the approach proposed in
110 the CROW-CUR report [22] the component related to the concrete cover was removed following the
111 philosophy of the German National Annex to EN 1992-1-1 [23].

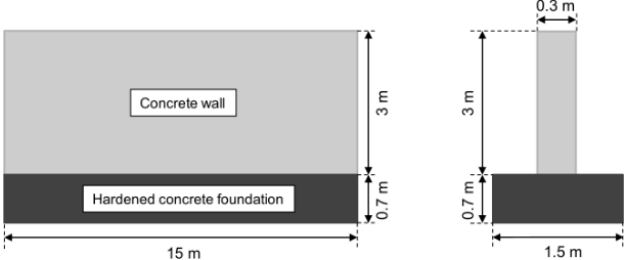
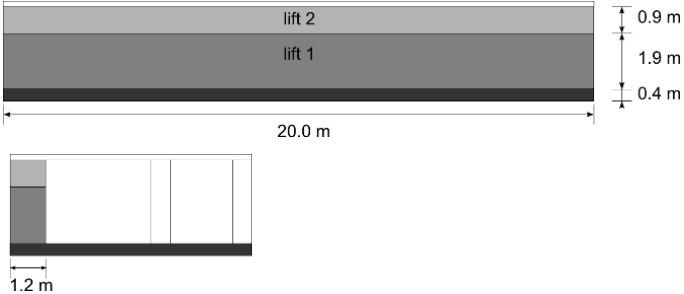
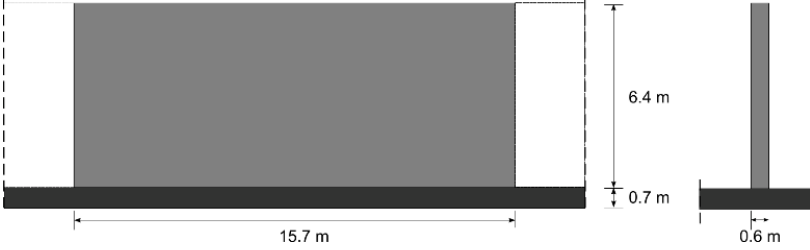
112 As mentioned earlier, a broader study based on in-situ measurements of the walls has been performed
113 by *Klemczak and Żmij* [10]. Nevertheless, new versions of the guidelines analysed in this study have
114 been issued which include significant modifications and thus deserve re-addressing. Most importantly,
115 however, the focus of this comparative study was rather on the easiness of use, not the physical
116 background of the model assumptions. Regarding the methods which are derived from the assumption
117 of crack-formation stage, comparative studies were performed by *Carino and Clifton* [24] for the

118 methods of *Gilbert* [25] (implemented in CIA Z7/06 [16]) and *Base and Murray* [26] (whose modified
119 version is implemented in AIJ-SRC recommendations [16]) but only for the end-restrained elements.
120 The modified Base–Murray method implemented in AIJ-SRC guideline, which is the only example of
121 the method developed originally for the elements under imposed strains accounting for the stage of
122 cracking, has never been compared with the modified methods originating from the models for the
123 elements under direct tension (Eurocode 2 and ACI 207/224). This leaves an open question whether its
124 mechanically sound philosophy makes this approach superior to the other methods regarding its
125 performance in crack width estimation.

126 Therefore, in this paper a *benchmark* type of investigation has been performed with the aim to evaluate
127 the discrepancies in the restraint-induced crack width calculated from different codified models around
128 the world. First, estimates of the crack width for given reinforcement as well as the required
129 reinforcement to limit the crack width were made on a theoretical example of a wall-on-slab structure;
130 this also allowed to perform a sensitivity analysis of the methods. Second, the methods were validated
131 against two real-life case studies, which were comprehensively monitored for temperature, strains and
132 crack characteristics: a nuclear containment wall and a tank wall segment. Table 1 summarises the
133 analysed benchmark case studies – their nature and key takeaway conclusions.

134 The aim of this research was therefore to perform an integrative analysis of several approaches which
135 are intended to be inherently wide yet relatively simple to use for design purposes, and consequently to
136 reach global understanding of the phenomenon of restraint-induced cracking. As an effect, the authors
137 define the ranges of applicability of the currently used models and their limitations, providing useful
138 guidelines for the design with the use of these models, given the particularities of the design of the
139 structures subjected to the restraint of imposed strains. Moreover, a sound and solid basis is built for
140 conceptualisation of new models, whose development is needed to overcome the deficiencies of the
141 current solutions, such as the proposals of *Schlicke* et al. [27], *Tan* et al. [28] or *Somma* et al. [29].

Table 1. Summary of the analysed case studies.

CASE STUDY	Nature of the example and level of information available	Purpose of the study
<p>Wall-on-slab structure (Section 3)</p> 	<p>Theoretical example representing a typical semi-massive base-restrained wall on foundation. All the input data are assumed as realistic probable values. This example is used for comparative study and sensitivity analysis of the analysis methods.</p>	<p>Basic understanding of differences of in the analysed models.</p>
<p>Massive wall of Civaux NPP mock-up (Section 4)</p> 	<p>Real-life case study. Only early-age cracking (due to hydration and early shrinkage). Input data: geometry, materials, reinforcement, measurements of temperature (in-situ) and shrinkage (laboratory), measurements of crack spacing and crack width after 5 days.</p>	<p>Predictive capacity of the models in estimation of the magnitude of early-age imposed strains, crack spacing and crack width in crack-formation stage. Study on the influence of massivity/cross-sectional dimensions.</p>
<p>Heavily reinforced tank wall segment (Section 5)</p> 	<p>Real-life case study. Cracking due to both early-age and long-term imposed strains. Input data: geometry, materials, reinforcement, measurements of total strains (in-situ), temperature (in-situ), shrinkage (laboratory), crack spacing and crack width after 16 days, 90 days and 9 months.</p>	<p>Predictive capacity of the models in estimation of the crack spacing and crack width change in time (from early-age to long-term) with changing imposed strains.</p>

143 2 Restraint-induced cracking in edge-restrained elements

144 2.1 Characterisation of cracking in walls

145 Cracking behaviour of edge-restrained structures, such as walls on slabs, have been characterised by
146 the authors based on a study of a collection of real-life examples of cracked wall-on-slab structures [1].
147 The stresses in these structural elements are generated due to eccentric restraint of potential
148 elongation/shortening of the wall by the restraining element (foundation or other adjacent element, e.g.,
149 neighbouring segment or lift). The decisive stress distribution varies throughout the structure and
150 depends on the magnitude of the imposed strains in the wall, stiffness ratios between the wall and
151 restraining body as well as the length-to-height ratio of the wall, i.e., a ratio relevant to a potential
152 cracking pattern. When the tensile capacity of concrete of the wall is reached, tensile stresses lead to
153 formation of cracks. In the simplest case of a base-restrained element, the first crack appears
154 theoretically at half length of the wall, near the joint with the underlying foundation, and develops
155 toward the top edge of the wall. This crack can be followed by other cracks, which appear at a certain
156 distance from one another and reach a certain height. The final cracking pattern depends on the number
157 of factors including those described before, as well as on the support conditions (number of restrained
158 edges). The following factors were identified to influence the cracking potential and cracking pattern
159 in the edge-restrained elements subjected to imposed strains [1]:

- 160 1. **Massivity of the element** which is a measure of proneness of the structure to either thermal or
161 shrinkage cracking as well as of the share of self-induced and restraint stresses in the crack risk
162 assessment and cracking pattern characterisation.
- 163 2. **Mix composition** which in combination with the massivity of the element and curing conditions,
164 influences the magnitude of the imposed strains at early age. Optimum mix design is of special
165 importance in externally-restrained elements due to the inherent trade-off between decreasing the
166 imposed strains – especially thermal strains – and maintaining relatively fast development of
167 strength.

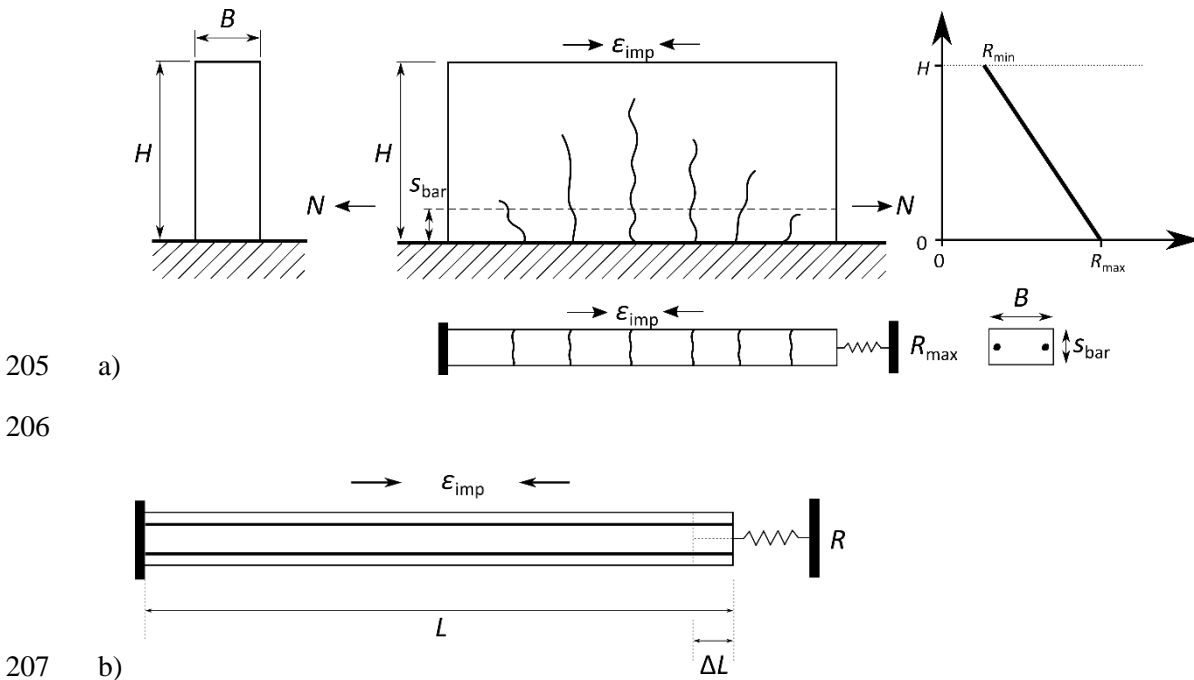
- 168 3. **Degree of external restraint** which determines the magnitude of stress-effective (restrained) part
169 of imposed strain, expressed by means of the length-to-height ratio of the restrained element as
170 well as its relative stiffness with respect to the restraining element.
- 171 4. **Support conditions** – the number of restrained edges – which determines the pattern of cracks:
172 their location, range, spacing and shape. For the base-restrained elements, cracks are vertical and
173 the highest along the centreline and decrease in height and slant towards free edges. The number
174 of restrained edges (base only / base + 1 side / base + 2 sides) has no direct effect on the width of
175 the cracks, only influences their amount and range.
- 176 5. **Reinforcement** – horizontal reinforcement is of interest for restraint-induced cracking in walls.
177 Naturally, higher reinforcement ratio allows to limit the width of the cracks and their spacing,
178 however, the efficiency of reinforcement in limiting the crack widths decreases with an increasing
179 reinforcement ratio. Furthermore, for low reinforcement ratios ($< 0.7\%$), especially close to the
180 minimum reinforcement, high variability and randomness of crack widths is observed, as the
181 activated reinforcement in the vicinity of the crack may reach very high strains with significant
182 deterioration of bond properties and there is no control of cracking.

183 2.2 Crack width estimation in design guidelines

184 The crack width in an edge-restrained element can basically be expressed by the product of the length
185 in which concrete slips on the reinforcement at both sides of the crack ($2l_e$), and the difference of the
186 mean strain between steel and concrete ($\varepsilon_{sm} - \varepsilon_{cm}$), which is referred to as the crack-inducing strain,
187 ε_{cr} . The same bond strength is assumed regardless of the stage of cracking (crack formation stage or
188 stabilised cracking stage) as well as that stabilised crack spacing is reached when $s_r = 2l_e$. That is why
189 the component of twice the transfer length is often simplified by the crack spacing. In edge-restrained
190 elements, cracking changes internal forces only locally and the strain difference depends on the
191 restrained part of strain of the uncracked section. Consequently, the value of the crack-inducing strain
192 is expressed the part of the restrained strain that is relieved by forming cracks and is equal to the
193 restrained part of imposed strain $\varepsilon_{rest} = R \cdot \varepsilon_{imp}$ minus the average tensile strain in the concrete after
194 cracking, which is related to the portion of its tensile capacity $k_t \cdot \varepsilon_{ctu}$:

195
$$w = s_r \cdot (\varepsilon_{sm} - \varepsilon_{cm}) = s_r \cdot \varepsilon_{cr} = s_r \cdot (\varepsilon_{rest} - k_t \cdot \varepsilon_{ctu}) \quad (1)$$

196 Table 2 summarises the formulas in the crack width calculations for edge-restrained elements with
 197 different standardised methods, discussed in [12]. In all cases crack spacing is derived from the model
 198 of a tie: the edge-restrained elements are represented as ties in which the fixation at the extremities is
 199 replaced with an actual degree of restraint described with the restraint factor. This is graphically
 200 explained in Fig. 1a. Majority of the methods treat the whole wall as a single tie and use the maximum
 201 value of the restraint factor at the height for the design. ACI 207.2 [8] acknowledges the fact that the
 202 degree of restraint in an edge-restrained element decreases towards the free edge and allows to
 203 differentiate the required reinforcement ratio at the height of the wall by dividing the wall into sub-ties
 204 (lifts) with decreasing value of the restraint factor.



208 **Figure 1.** Graphical explanation of the method for SLS design of cracking of edge-restrained elements subjected
 209 to imposed deformations with the use of an equivalent tie model: (a) definition of the model; (b) compatibility of
 210 deformations.

211 **2.3 Degree of restraint and restraint factor**

212 One of the key parameters in crack width control of edge-restrained elements is the degree of restraint
 213 conventionally represented with a restraint factor, R . Discrepancies can be noted between the methods
 214 in the definition of the degree of restraint and restrained part of strain, especially in the meaning of ε_{imp}

215 and $\varepsilon_{\text{free}}$. Therefore, the authors found it crucial to unify the denotations throughout the methods in this
216 paper to facilitate their use for the designer. These unified denotations have been introduced in Fig. 1b,
217 and used in the presentation of the methods in Table 2 and throughout the paper.

218 Figure 1b illustrates the conditions of deformations compatibility in a partially-restrained tie which is
219 subjected to imposed strain ε_{imp} . The source of this imposed strain might be temperature drop and/or
220 shrinkage of concrete. Due to partial restraint of the element, a part of this strain will cause deformation
221 of an element, and a strain related to this deformation is a free part of imposed strain, $\varepsilon_{\text{free}} = \Delta L/L$.
222 The remaining part of the strain is, in turn, a restrained strain $\varepsilon_{\text{rest}}$, so $\varepsilon_{\text{imp}} = \varepsilon_{\text{free}} + \varepsilon_{\text{rest}}$. The
223 magnitude of the restrained strain depends on the degree of restraint, R , which can thus be defined as:

$$224 \quad R = \frac{\varepsilon_{\text{rest}}}{\varepsilon_{\text{imp}}} = \frac{\varepsilon_{\text{imp}} - \varepsilon_{\text{free}}}{\varepsilon_{\text{imp}}} = 1 - \frac{\varepsilon_{\text{free}}}{\varepsilon_{\text{imp}}} \quad (2)$$

225 Hence, with the use of the degree of restraint, the restrained part of imposed strain can be expressed as
226 $\varepsilon_{\text{rest}} = R \cdot \varepsilon_{\text{imp}}$.

227 **Table 2.** Summary of the methods for crack width calculation in edge-restrained elements with different guidelines [12].

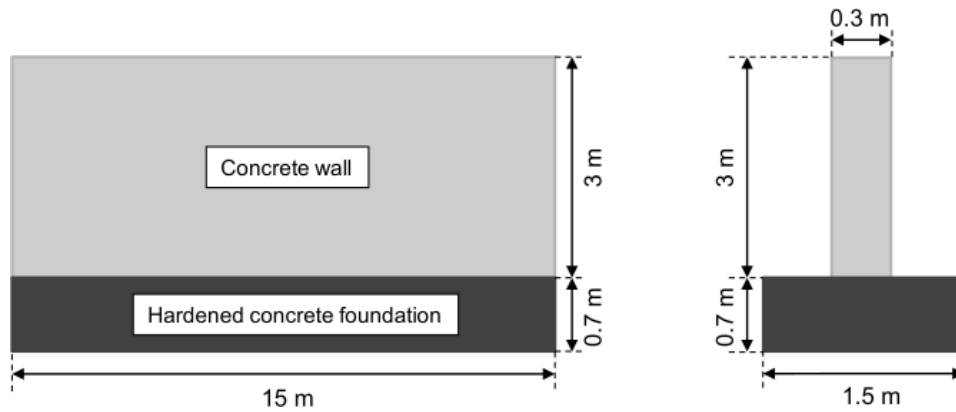
code	crack spacing s_r	crack-inducing strain $\varepsilon_{cr} = \varepsilon_{sm} - \varepsilon_{cm}$	crack width
EN 1992-1-1:2004 & EN 1992-3:2006	$s_{r,max} = 3.4 \cdot c + 0.425 \cdot k_1 \cdot k_2 \cdot \frac{\phi}{\rho_{eff}}$ $k_1 = 0.8$ for good bond	$\varepsilon_{cr} = \varepsilon_{rest} = R_{ax} \cdot \varepsilon_{imp}$	$w_{max} = s_{r,max} \cdot (\varepsilon_{sm} - \varepsilon_{cm})$
CIRIA C766	$s_{r,max} = 3.4 \cdot c + 0.425 \cdot k_1 \cdot k_2 \cdot \frac{\phi}{\rho_{eff}}$ $k_1 = 1.14$ for poor bond (at early age)	$\varepsilon_{cr} = \varepsilon_{rest} - 0.5\varepsilon_{ctu} = R \cdot \varepsilon_{imp} - 0.5\varepsilon_{ctu}$ $= K_{c1} \cdot R_1 \cdot [\varepsilon_{T1} + \varepsilon_{ca}(3)] + K_{c2} \cdot R_2$ $\cdot [\varepsilon_{T2} + \varepsilon_{ca}(28) - \varepsilon_{ca}(3)] + K_{c2} \cdot R_3 \cdot \varepsilon_{ca} - 0.5\varepsilon_{ctu}$ where $\varepsilon_{ctu}(t) = \frac{f_{ct,0.05}(t)}{E_{cm}(t) \cdot K_c}$	$w_{max} = s_{r,max} \cdot (\varepsilon_{sm} - \varepsilon_{cm})$
EN 1992-1-1:2023	$s_{rm} = 1.5 \cdot c + \frac{k_{fl} \cdot k_b}{7.2} \cdot \frac{\phi}{\rho_{eff}} \leq \frac{1.3}{k_w} (h - x)$ $k_w = 1.7$	$\varepsilon_{cr} = \varepsilon_{rest} - k_t \cdot \varepsilon_{ctu} = R_{ax} \cdot \varepsilon_{imp} - k_t \cdot \varepsilon_{ctu}$ $= R_{ax,1} \cdot [\varepsilon_{T1} + \varepsilon_{ca}(t)] + R_{ax,2} \cdot \varepsilon_{T2} + R_{ax,3} \cdot \varepsilon_{ca}(t) - k_t \varepsilon_{ctu}$ where $\varepsilon_{ctu}(t) = \frac{f_{ctm}(t)}{E_{cm}(t)}$ and $k_t = 0.6$	$w_{max} = k_w \cdot s_{rm} \cdot (\varepsilon_{cm} - \varepsilon_{sm})$ $= s_{r,max} \cdot (\varepsilon_{sm} - \varepsilon_{cm})$
CIA Z7/06	$s_{r,max} = 3.4 \cdot c + 0.425 \cdot k_1 \cdot k_2 \cdot \frac{\phi}{\rho_{eff}}$ $k_1 = 1.14$ for good bond	$\varepsilon_{cr} = \varepsilon_{rest} - \varepsilon_{ctu} = R \cdot \varepsilon_{imp} - \varepsilon_{ctu}$ where $\varepsilon_{rest} = \sigma_{cs}/E_{c,eff}$ and $R = \varepsilon_{rest}/\varepsilon_{imp}$	$w_{max} = s_{r,max} \cdot (\varepsilon_{sm} - \varepsilon_{cm})$
AIJ-SRC	transfer length: $2l_e = 0.1 \frac{\phi}{\rho}$ crack spacing: $s_{rm} = \frac{l}{m} \geq 2l_e$ where $m = 1 + \frac{L \cdot \alpha_e \cdot \rho}{2 \cdot l_e} \cdot \left(\frac{R \cdot \varepsilon_{imp} - \varepsilon_{ctu}}{b \cdot \varepsilon_{ctu}} \right)$	not determined explicitly ε_{imp} is limited to drying and autogenous shrinkage	$w_{mean} = 2l_e \left(\frac{\sigma_s}{E_s} + \frac{R \cdot \varepsilon_{imp}}{b} \right)$ R represents the actual degree of restraint in a wall
ACI 207.2 & 224	$s_{r,max} = \frac{w}{1.5 \cdot (R \cdot \varepsilon_{imp} - \varepsilon_{ctu})}$ based on the known crack width	$\varepsilon_{cr} = \varepsilon_{rest} - \varepsilon_{ctu} = R \cdot \varepsilon_{imp} - \varepsilon_{ctu}$	$w_{max} = 0.0145 \cdot \sigma_s \cdot \sqrt[3]{a_s \cdot A_{c,eff}} \cdot 10^{-3}$

where:			
		R	restraint factor (from linear analysis)
a_s	distance from tensioned edge of section to centre of gravity of reinforcement	R_{ax}	restraint factor accounting for creep
c	concrete cover	α_e	ratio of moduli of elasticity of steel and concrete
f_{ct}	tensile strength of concrete	ρ	reinforcement ratio
$f_{ctk,0.05}$	5%-quantile characteristic tensile strength of concrete	ρ_{eff}	effective reinforcement ratio
f_{ctm}	mean tensile strength of concrete	σ_s	stress in reinforcement
k_i	coefficients	ϵ_{ca}	autogenous shrinkage strain
l_e	transfer length	ϵ_{cd}	drying shrinkage strain
s_0	slip length, $s_0 = 2l_e$	ϵ_{cm}	mean strain in concrete
s_{rm}	mean crack spacing	ϵ_{cr}	crack-inducing strain in edge-restrained element
$s_{r,max}$	maximum crack spacing	ϵ_{ctu}	tensile capacity of concrete
w_{mean}	mean crack width	ϵ_{free}	free (unrestrained) part of imposed strain
w_{max}	maximum crack width	ϵ_{imp}	imposed strain (thermal, shrinkage)
$A_{c,eff}$	effective tensile area of concrete	ϵ_{rest}	restrained part of imposed strain
$E_{c,eff}$	effective modulus of elasticity of concrete	ϵ_{sm}	mean strain in reinforcement
E_s	modulus of elasticity of steel	ϵ_T	thermal strain
K_c	coefficient taking into account the effect of creep	ϕ	diameter of reinforcement

229 **3 Demonstration example**

230 **3.1 Data**

231 The case is a concrete wall cast on a rigid foundation. A schematic diagram of the investigated case is
 232 shown in Fig. 2 while Table 3 enlists the data assumed for the analysis.



233
 234 **Figure 2.** Layout of the hypothetical case study for a wall cast on rigid foundation.

235 **Table 3.** Input parameters for cracking models for a demonstration example.

Limit surface crack width [mm]	0.3
Strength class according to EN 1992-1-1:2004 [5]	C30/37
Cement type according to EN 206 [30]	CEM II 32.5R
Characteristic compressive strength of concrete f_{ck} [MPa]	30
Yield strength of reinforcing steel f_{yk} [MPa]	500
Elastic modulus of reinforcing steel E_s [GPa]	200
Thermal dilation coefficient of concrete and steel [$\mu\epsilon/^\circ\text{C}$]	10
Cover to reinforcement [mm]	40
Early-age temperature drop [$^\circ\text{C}$]	20
Long-term temperature change [$^\circ\text{C}$]	20
Total free autogenous shrinkage [$\mu\epsilon$] $\epsilon_{ca,\infty}$	50
Total free drying shrinkage [$\mu\epsilon$] $\epsilon_{cd,\infty}$	300

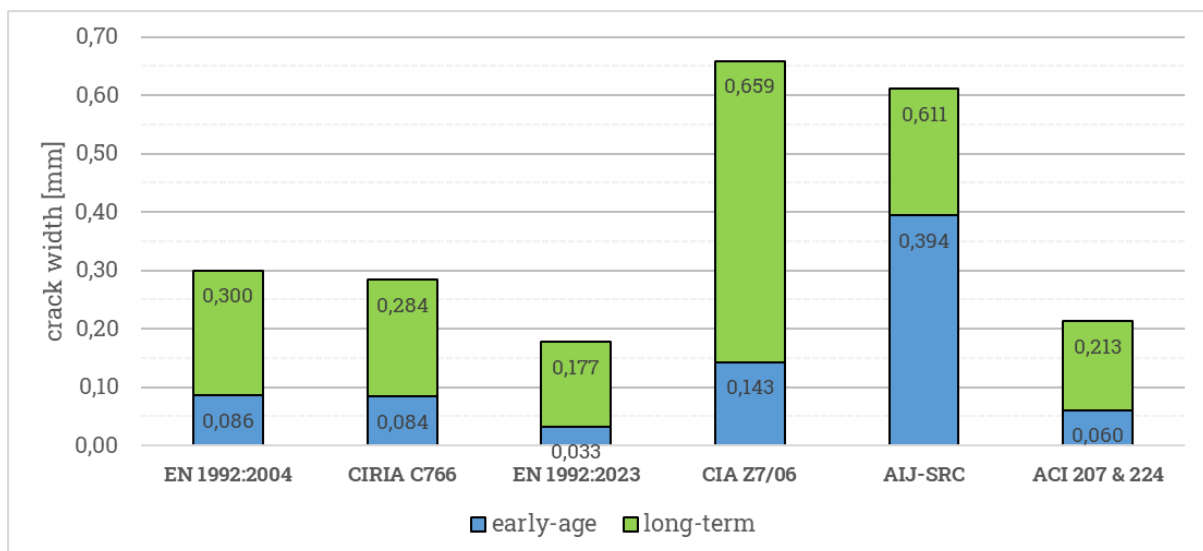
236 It was assumed that both the wall and foundation were made of the same C30/37 class concrete, with
 237 the characteristic compressive strength of 30 MPa according to EN 1992-1-1:2004 [5] which value was
 238 used for calculations with all the methods. The concrete mix was assumed to be composed of CEM II
 239 32.5R cement and natural quartzite aggregate. This type of cement was classified as “ordinary” cement

240 according to the AIJ-SRC recommendations [16] and as “Type I” cement according to the ACI Report
 241 209 [31]. The analysed wall was cast 28 days after the foundation and it was assumed that at the time
 242 of casting of the wall the concrete of the foundation has achieved its mature properties.

243 All the values of imposed deformations were estimated with CIRIA C766 [15] to provide realistic values
 244 representative for the analysed case. To maintain consistency throughout the methods, the age of
 245 concrete for the early-age analysis was taken as 3 days. The autogenous shrinkage strain at after 3 days
 246 was taken as $15 \mu\epsilon$ following EN 1992-1-1:2004 [5]. The drying shrinkage was taken as uniform in the
 247 cross-section (a mean value of $300 \mu\epsilon$) and the effect of self-equilibrating stresses induced by the actual
 248 variation of shrinkage in the cross-section were taken into account indirectly, if allowed for in a model.

249 3.2 Results and discussion

250 In the first step, the crack width was calculated for given reinforcement. The applied reinforcement ($\phi 12$
 251 bars spaced by 160 mm placed symmetrically at both sides of the wall; reinforcement ratio of 0.47%)
 252 was determined with the method of EN 1992-1-1:2004 & EN 1992-3:2006 to limit the final width of
 253 the crack to $w_{lim} = 0.3$ mm. Figure 3 shows comparison between the crack width obtained with each
 254 method for this reinforcement. Detailed intermediate results are listed in Table 4. In the second step of
 255 calculations, each method was used to calculate the reinforcement required to limit the final crack width
 256 to $w_{lim} = 0.2$ mm, 0.3 mm and 0.4 mm. The results are presented in Fig. 4.



257
 258 **Figure 3.** Comparison between crack width estimations in a demonstration example of a wall for given
 259 reinforcement ($\phi 12$ cc 160 mm) with different standardised methods.

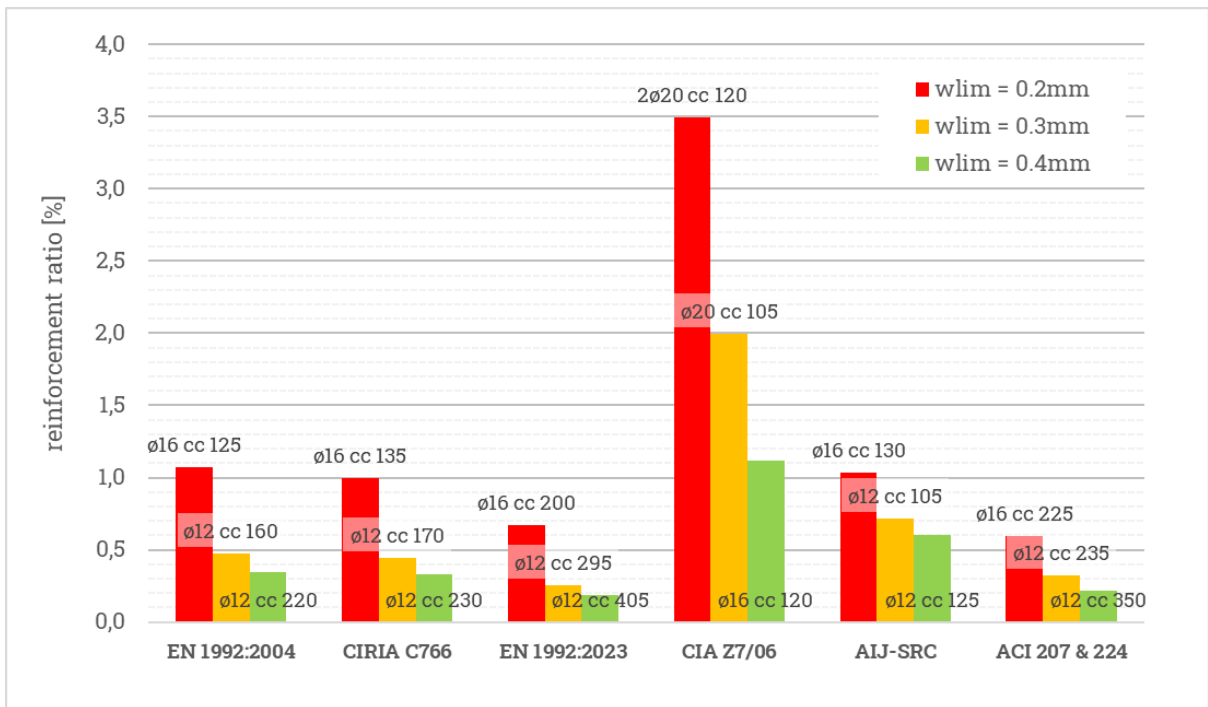
Table 4. Details of crack width calculations for a demonstration example with different standardised methods.

property	EN 1992-1-1:2004 & EN 1992-3:2006	CIRIA C766	EN 1992-1-1:2023	CIA Z7	AIJ-SRC	ACI 207.2 & 224
$A_{c,eff}$ [cm ²]	1150	1150	1060	1500	1500	1500
ρ_{eff} [%]	0.61	0.61	0.67	0.47	0.47	0.47
EARLY-AGE CRACK WIDTH						
$f_{ct}(3)$ [MPa]	1.73	1.21	1.46	1.11	n/a	1.20
$E_c(3)$ [GPa]	27.4	27.4	21.9	20.1	20.4	17.5
φ_{ea}	0.55	0.54	0.55	0.55	0.55	n/a
$E_{c,eff}(3)$ [GPa]	17.7	17.8	14.1	13	13.2	17.5
ε_{imp-ea} [$\mu\varepsilon$]	214.6	214.6	194.6	214.6	214.6	214.6
ε_{ctu-ea} [$\mu\varepsilon$]	63.3	68.1	66.8	55.2	75.1	100.0
$s_{r,max-ea}$ [cm]	80.0	108.4	56.9	137.3	375**	256.3***
R at early age	0.50*	0.80	0.50*	0.74	0.80	0.63
$\varepsilon_{rest-ea}$ [$\mu\varepsilon$]	107.3	111.6	97.3	159.0	n/a	135.8
ε_{cr-ea} [$\mu\varepsilon$]		77.6	57.2	103.8		35.8
w_{ea} [mm]	0.086	0.084	0.033	0.143	0.394	0.060
LONG-TERM CRACK WIDTH						
$f_{ct}(\infty)$ [MPa]	2.9	2.03	2.9	1.97	n/a	2.73
$E_c(\infty)$ [GPa]	32	32	32	29.6	25.3	25.9
φ_{lt}	1	1	1	1	1	n/a
$E_{c,eff}(\infty)$ [GPa]	16	16	16	14.8	12.6	25.9
ε_{imp-lt} [$\mu\varepsilon$]	750.0	750.0	730.0	750.0	750.0	750.0
ε_{ctu-lt} [$\mu\varepsilon$]	90.6	126.9	90.6	66.7	114.8	150.0
$s_{r,max-lt}$ [cm]	80.0	108.4	56.9	137.3	136.4**	55.8***
R in long term	0.50*	0.80	0.50*	0.73	0.80	0.54
		0.80	0.50*			
$\varepsilon_{rest-lt}$ [$\mu\varepsilon$]	375.0	325.8	365.0	546.4	n/a	403.8
ε_{cr-lt} [$\mu\varepsilon$]		262.3	310.6	479.4		253.8
w_{lt} [mm]	0.300	0.284	0.177	0.659	0.611	0.213

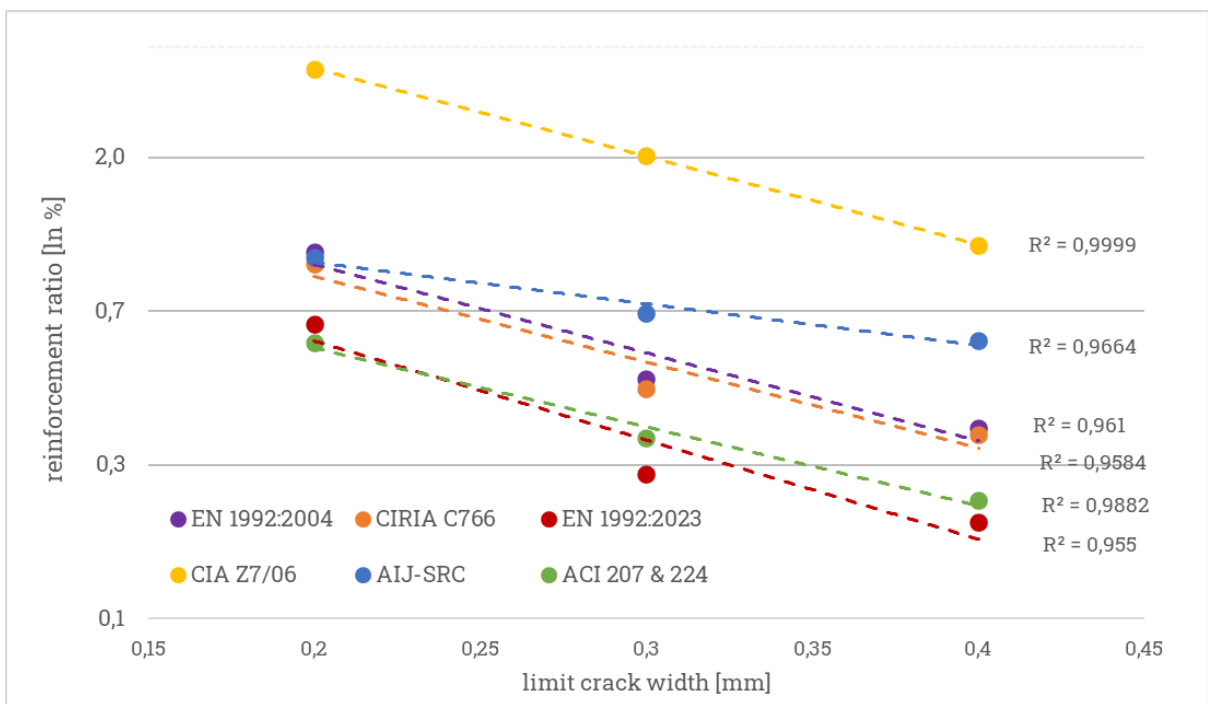
* accounts for creep

** mean crack spacing (in crack-formation phase) to be multiplied by 1.7 to convert w_{mean} to w_{max}

*** calculated from the crack width



261 a)



262 b)

263 **Figure 4.** Comparison between reinforcement required to limit the long-term (final) crack width in a
 264 demonstration example with different standardised methods.

265 3.2.1 EN 1992-1-1 and related documents

266 Comparing the European methods, i.e. past version of EN 1992-1-1:2004 [5] and EN 1992-3:2006 [6],
 267 CIRIA C766 [15] and new version of EN 1992-1-1:2023 [14], it can be observed that for the same
 268 applied reinforcement the obtained width of the crack decreases (Fig. 3). Naturally, analogical

269 observation can be made when comparing the reinforcement ratios required to limit the crack widths
270 (Fig. 4). For each analysed scenario the greatest area of the required reinforcement is predicted by EN
271 1992-1-1:2004 & EN 1992-3:2006 method, followed by the CIRIA C766 and then EN 1992-1-1:2023
272 approaches. One may infer that the guidelines of CIRIA C766 and EN 1992-1-1:2023 by proposing
273 modifications to the method of EN 1992-1-1:2004 & EN 1992-3:2006 aim at providing more
274 economical and sustainable design solutions. This is predominantly attributed to the lower value of the
275 crack-inducing strain, which in case of CIRIA C766 and EN 1992-1-1:2023 takes into account concrete
276 extensibility (strain relief) after cracking (see Table 4).

277 The predicted value of the crack-inducing strain is higher at early-age (77.6 vs. 57.2 $\mu\epsilon$) but lower in
278 long-term (262.3 vs. 310.6 $\mu\epsilon$) with the method of CIRIA C766 in comparison to EN 1992-1-1:2023.
279 Although the methods of CIRIA C766 and EN 1992-1-1:2023 use the same philosophy for
280 determination of this strain, there are two important factors responsible for the difference. First, in EN
281 1992-1-1:2023 the effect of creep on the reduction of stresses is already accounted for in the value of
282 the degree of restraint, and by default there is no differentiation proposed to be made between its early-
283 age ($R_{ax,1}$) and long-term ($R_{ax,2}$ and $R_{ax,3}$) values. In the early-age analysis the default recommended
284 values of the restraint factors according to both methods are almost equal (0.5 in EN 1992-1-1:2023 vs.
285 $0.8 \cdot 0.65 = 0.52$ in CIRIA C766). The free strain, however, is lower by EN 1992-1-1:2023 (194.6 vs.
286 214.6 $\mu\epsilon$ in CIRIA C766) as the standard allows for the reduction of the early-age thermal strain to
287 account for the positive effect of compressive stresses in heating phase ($0.9\epsilon_{T1}$). In the long-term
288 analysis, in turn, the effective restraint factor by CIRIA C766 is lower ($0.8 \cdot 0.5 = 0.4$ in comparison to
289 0.5 by EN 1992-1-1:2023) due to the higher effect of creep, thus the restrained part of strain is also
290 lower.

291 A comment must be made, however, about the restraint factor value used in the calculations. Numerous
292 discussions have been made, also by the authors [1, 12], about the challenges in determination of the
293 decisive degree of restraint for crack width calculations in wall-on-slab structures. In this study default
294 values proposed by the standards were used. However, some of the guidelines provide detailed
295 recommendations for more precise calculation of the degree of restraint. CIRIA C766 refers in this
296 regard to the proposal of ACI 207 to calculate the axial restraint factor as:

297
$$R = \frac{1}{1 + \frac{A_c E_c}{A_f E_f}} \quad (3)$$

298 The value of the restraint factor calculated with this proposal gives by far the lowest values (0.63 and
 299 0.54 at early-age and long-term, respectively – see Table 4), yet it is the maximum value at the wall–
 300 foundation joint, while the decisive location where the maximum crack width is expected lies
 301 somewhere above the joint. CIRIA C766 suggests this level to be $0.1L$, for which the expected restraint
 302 factor at given height h calculated following CIRIA C766 recommendations:

303
$$R(h) = R \cdot \left[\left(1.372 \cdot \left(\frac{h}{L} \right)^2 - 2.543 \cdot \frac{h}{L} + 1 \right) + 0.044 \cdot \left(\frac{L}{H} - 1.969 \right) \cdot \left(\frac{h}{H} \right)^{1.349} \right] \quad (4)$$

304 would be even lower, 0.51 and 0.44 at early-age and in long term, respectively.

305 EN 1992-1-1:2023 also allows for more sophisticated methods to be used, e.g. by determining the
 306 degree of restraint through (linear) finite element analysis; the restraint factor could be then calculated
 307 acc. to the Eq. (2). EN 1992-1-1:2023. Such an approach seems reasonable especially in case of
 308 geometrically complex structures for which simplified methods of determination of the restraint factor
 309 cannot be applied. In this regard, the authors refer the reader to the RILEM TC 287-CCS
 310 recommendations **Erreur ! Source du renvoi introuvable.** for detailed explanation of FEM-based
 311 modelling of structures subjected to imposed strains. For the structures with simpler geometries, such
 312 as the ones analysed in the paper, guidance of other standards or recommendations can be used. Such
 313 provisions are given, as already mentioned, by ACI 207.2 and CIRIA C766, but also non-standardised
 314 solutions exists, which have been discussed in e.g. [32]. Creep relaxation can be also accounted for
 315 independently in accordance with Annex D; the influence of concrete age and creep on stress values is
 316 taken into account by the effective elastic modulus of concrete, i.e. simplified viscoelastic model.

317 Secondly, CIRIA C766 accounts additionally for higher level of strain relief ($k_t \varepsilon_{ctu}$ component) in long
 318 term than EN 1992-1-1:2023 (63.4 vs. 54.4 $\mu\epsilon$). CIRIA C766 increases tensile capacity of concrete
 319 under sustained loading by accounting for the effect of creep (which is not done in EN 1992-1-1:2004
 320 and EN 1992-1-1:2023, where tensile capacity is determined under the assumption of the short-term
 321 character of the load – see Table 4). Even though the tensile capacity of concrete according to CIRIA
 322 C766 is calculated using the characteristic tensile strength $f_{ct,0.05}$, the age-adjusted modulus of

323 elasticity of concrete $E_{c,eff}$ is applied. The level of increase is by 8% at early-age and by 40% at long-
324 term in comparison to the scenario in which mean tensile strength and modulus of elasticity are
325 considered.

326 However, even though the crack-inducing strain is the lowest according to CIRIA C766, the final width
327 of the crack is the lowest based on EN 1992-1-1:2023. This results, in turn, from the crack spacing
328 which is estimated to be twice the value of EN 1992-1-1:2023 by CIRIA C766 (108 vs. 57 cm). In
329 tensioned elements, as the ones studied in this paper, for the same geometry and reinforcement, the
330 crack spacing calculated with the formula of EN 1992-1-1:2023 gives lower values than by the past
331 version of EN 1992-1-1:2004 due to, among the others, reduced impact of concrete cover and favourable
332 effects of bond (coefficient k_1 takes the value of ~0.55 in EN 1992-1-1:2023 in comparison to 0.8 acc.
333 to EN 1992-1-1:2004). CIRIA C766, however, states that the bond properties at early-age are poor and
334 recommends that the value of k_1 should be increased ($k_1 = 0.8/70\% = 1.14$).

335 If the three methods (of EN 1992-1-1:2004 & 1992-3:206, CIRIA C766 and EN 1992-1-1:2023) were
336 consistent in their assumptions of relevant parameters, i.e. if the value of the modulus of elasticity was
337 reduced by creep and by assuming poor bond between the steel and reinforcement ($k_1 = 1.14$), the
338 observed tendency when comparing the methods would be further enforced. The predicted final width
339 of the crack would be respectively equal to 0.325 mm (EN 1992-1-1:2004 & 1992-3:2006), 0.284 mm
340 (CIRIA C766) and 0.159 mm (EN 1992-1-1:2023).

341 **3.2.2 CIA Z7/06 recommendations**

342 The method of CIA Z7/06 [16] gives by far the greatest width of the crack in the wall (its value is over
343 twice the target limit value of 0.3 mm, so the width of the crack predicted by EN 1992-1-1:2004 &
344 1992-3:2006 – see Fig. 3). This should be attributed to the crack spacing and restrained part of strain.

345 The spacing of the cracks is calculated after CIRIA C766 (i.e. with the formula of EN 1992-1-1:2004
346 but with poor bond assumption $k_1 = 1.14$, see Table 2). The crack spacing is further increased by
347 decrease in the effective reinforcement ratio: in the method of CIA Z7/06 the effective tensile area of
348 concrete is not limited as in EN 1992-1-1:2004, but the whole tensioned cross-section is considered.

349 Regarding the restrained part of strain, in the method of CIA Z7/06 the restraint factor is calculated

350 from the geometry and stiffness of the wall and foundation. Therefore, the restraint factor obtained with
351 this method has the meaning of R factor from CIRIA C766 rather than that of R_{ax} from EN 1992-
352 3:2006. Consequently, the effect of strain reduction by creep is not taken into account in this method.
353 Finally, the CIA Z7 methods takes into consideration the effect of strain relief, in contrary to EN 1992-
354 1-1:2004.

355 If good bond was assumed ($k_1 = 0.8$), the expected widths of the cracks would decrease from 0.143 mm
356 and 0.659 mm (see Fig. 3) to 0.104 mm and 0.481 mm (i.e. by 27%) for early-age and long-term,
357 respectively. Furthermore, if the tensile area was further reduced according to the recommendations of
358 EN 1992-1-1:2004 to the effective area $A_{c,eff}$ (from 1500 to 1150 cm²), the resultant widths of the cracks
359 would be reduced to 0.083 mm and 0.384 mm (i.e. by 42%), respectively. It must be noted that the
360 analysed element is relatively thin, so the range of impact of the reinforcement is high ($h_{c,eff}$ by EN
361 1992-1-1:2004 is 77% of $0.5h$). Thus, with an increasing thickness of the element the influence of the
362 effective reinforcement ratio would be increasing. Finally, if the value of the restraint factors R
363 calculated with the method of CIA Z7/06 were reduced from 0.74 and 0.73 to 0.5 for early-age and 0.4
364 for long-term (to account for the reduction by creep as in EN 1992-1-1:2004 and CIRIA C766), the
365 resultant crack width would be reduced to 0.042 mm and 0.187 mm (i.e. by 72%), respectively.

366 **3.2.3 AIJ-SRC recommendations**

367 A comparably large final crack width was obtained with the AIJ-SRC method [16] (0.611 mm for a
368 long-term crack width – see Fig. 3), in addition to the fact that with this method the greatest early-age
369 crack width was predicted (0.394 mm). This method was derived from different assumptions than the
370 previous ones. First, it does not assume the stabilised crack spacing being reached. Therefore, the
371 calculated transfer length $s_0 = 2l_e$ is compared with the calculated crack spacing s_r , as it is expected
372 that in the crack-formation stage s_0 is smaller than the actual spacing of the cracks (this assumption has
373 been proven true in the course of calculations). Secondly, uniform spacing between the cracks is
374 considered when determining the stress in reinforcement, so the resultant width of the crack is a mean
375 width. For the sole purpose of this comparative study the crack widths obtained with the use of this
376 method were multiplied by 1.7 to convert them to the maximum values.

377 It is interesting to notice that according to the AIJ-SRC method the early-age crack width increases by
378 only 50% in long term (from 0.39 mm to 0.61 mm – see Fig. 3) while the strain is more than tripled
379 (free strain increases from 215 $\mu\epsilon$ to 750 $\mu\epsilon$ – see Table 4). This is opposite to the results of other
380 methods in which the crack width increase corresponds to the increase in strain. It is also worth
381 mentioning the amount of reinforcement required to limit the crack width according to AIJ-SRC method
382 in comparison to the CIA Z7/06 approach, which predicted comparably high widths of the crack. With
383 a comparable expected crack width of ~ 0.6 mm, it is enough to increase the reinforcement area by 50%
384 to reduce the crack width by half, while it must be increased 4 times to achieve the same effect according
385 to CIA Z7/06 (see Fig. 4). In general, the reinforcement requirements evaluated with the CIA Z7/06
386 approach are the highest for all the analysed limit crack widths. It is also interesting to notice that the
387 decrease in the required reinforcement with an increasing limit crack width predicted with CIA Z7/06
388 is practically linear while for all other methods the differences become smaller (reduction by \sim half
389 between 0.2 mm and 0.3 mm, and reduction by \sim quarter between 0.3 mm and 0.4 mm, as can be seen
390 in Fig. 4).

391 It must be emphasised that the method of AIJ-SRC modifies the original Base–Murray method [26]
392 derived from the model of a fixed tie (100% degree of restraint) by introduction of the restraint factor
393 to account for the partial restraint in the wall. However, it can be observed that the model is almost
394 insensitive to the degree of restraint (thus the restrained part of strain) until the stabilised crack spacing
395 is reached: increase in strain causes formation of new cracks, not the increase of the crack width. First
396 crack is predicted to be formed for the restraint factor of 0.2; by increasing the restraint factor up to 1,
397 the predicted number of cracks increases from 1 to 5 at early age and from 2 to 14 in long term, while
398 the change in the crack width is as little as from 0.36 mm to 0.42 and from 0.57 to 0.65, respectively.

399 **3.2.4 ACI reports 207.2 and 224**

400 In the method proposed in the ACI reports the maximum crack spacing is obtained from the mean
401 spacing with the conversion factor of 1.5 instead of 1.7. This procedure accounts also for the restraining
402 moment and its effect on the width of the crack. It must be emphasised that according to the approach
403 of the ACI reports the effect of creep is negligible, so the calculation procedure is based on the linear
404 elastic analysis.

405 The ACI 207.2 report [18] provides a method to determine the value of the restraint factor taking into
406 account the relative stiffness of the wall and foundation. It must be noted that the time-development of
407 the modulus of elasticity according to the ACI report [31] is significantly slower than according to other
408 methods, e.g. EN 1992-1-1:2004 [5], thus for the early-age analysis (after 3 days) the ratio between the
409 early-age and 28-days moduli is ~0.7 in comparison to ~0.9 for EN 1992-1-1:2004. The obtained values
410 of the restraint factor are visibly smaller than those obtained with the method of CIA Z7/06 (0.63 vs.
411 0.74 and 0.54 vs. 0.73 at early age and long term, respectively), and the highest value recommended by
412 CIRIA C766 (0.8) – see Table 4.

413 Additionally, the level of extensibility (strain relief related to tensile capacity of concrete) recommended
414 by ACI 207.2 report [18] is relatively high: 100 $\mu\epsilon$ at early age and 150 $\mu\epsilon$ in long term are the highest
415 values of all the methods. According to other methods, the tensile strain capacity can be calculated as a
416 ratio between the tensile strength and modulus of elasticity. If the tensile strain capacity was calculated
417 like that for the actual values of these mechanical properties as recommended by the ACI report, they
418 would be smaller: $\epsilon_{ctu} = f_{ct}/E_c = 71.2 \mu\epsilon$ and $105.3 \mu\epsilon$ for early-age and long-term. Consequently, the
419 early-age and long-term crack widths would increase from 0.060 mm and 0.213 mm (see Fig. 3) to
420 0.080 mm and 0.222 mm (by 33% and 4%), respectively. Finally, if the same value of the mean-to-
421 maximum crack width conversion factor ($\beta = 1.7$ instead of 1.5) was taken, these crack widths would
422 further increase to 0.084 mm and 0.229 mm (increase by 40% and 8%, respectively). These would still
423 be, however, one of the lowest predictions of crack widths obtained with the analysed methods.

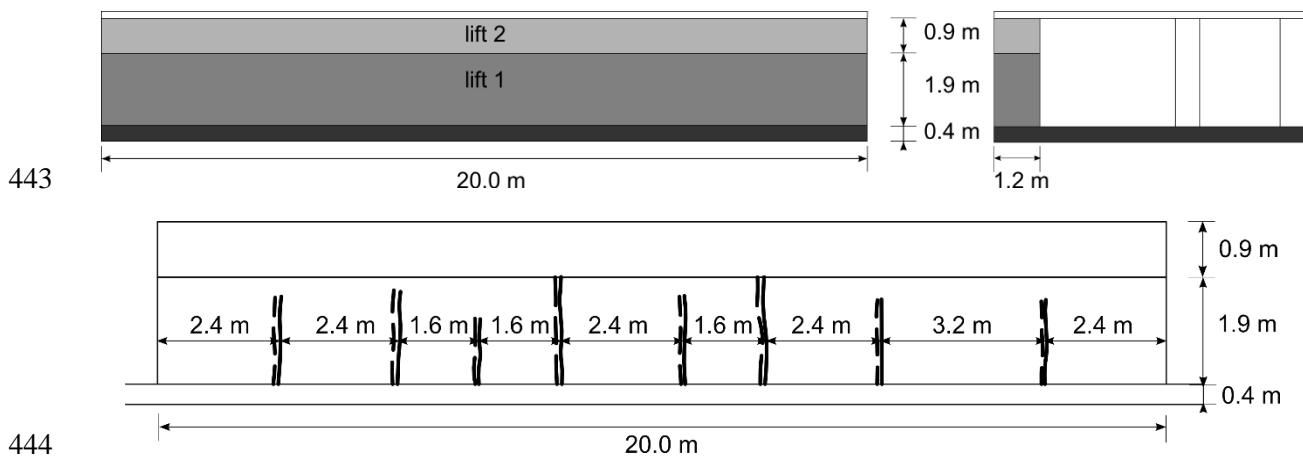
424 The required reinforcement ratios predicted with the ACI method is comparable with the predictions of
425 the EN 1992-1-1:2023; these two methods give the lowest required reinforcement ratios to limit the
426 crack widths (see Fig. 4). In the ACI approach this should be attributed to the positive effect of the
427 restraining along the edge of the wall which together with the reinforcement guarantees a sufficient
428 restraining moment, ensuring formation of a suitable number of cracks and by that reducing their widths.
429 A general comment can be made when analysing Fig. 4b about the effectiveness of the reinforcement
430 to limit the crack width. It can be concluded that all the methods reproduce the real-life observation
431 made by the authors in [1] that with increasing reinforcement ration the effectiveness in crack width

432 limitation decreases, i.e. the reinforcement requirements increase exponentially with a decrease of the
 433 limit crack width.

434 4 Case study 1: Massive wall of Civaux NPP mock-up

435 4.1 Description of the structure

436 The analysed wall was an experimental mock-up nuclear containment wall for a newly constructed
 437 nuclear power plant near Civaux, France, which can be classified as massive according to [34]. Figure
 438 5 schematically shows the geometry and cracking pattern in the wall. The data of the analysed case
 439 study are retrieved from the works [35], [36], [37], [38] and [39], and are presented in detail in Appendix
 440 A, sec. A.1. In the following sections the crack width calculations with the use of the studied methods
 441 are performed, and include comparison between the crack spacing, crack-inducing strain and predicted
 442 crack width.



443
 444
 445 **Figure 5.** Civaux mock-up wall: longitudinal view; cross-section; cracking pattern (crack widths 1×0.04 mm,
 446 4×0.1 mm, 2×0.2 mm and 1×0.5 mm).

447 4.2 Estimate of crack-inducing strain

448 Calculation of the crack-inducing strain requires determination of three components (see Table 2): (1)
 449 magnitude of imposed deformation induced by temperature variation and shrinkage ε_{imp} , (2) degree of
 450 restraint R and (3) tensile capacity ε_{ctu} . In the analysed case the cracking was caused by temperature
 451 variations due to simultaneous heating up of hardening concrete and its cooling to the ambient
 452 temperature, as well as autogenous shrinkage. As the wall was kept in formwork over the period of
 453 cooling, it could be assumed that drying was negligible.

454 Thermal strain was calculated as a product of temperature difference and coefficient of thermal dilation
455 of concrete $\varepsilon_T = \alpha_T \cdot \Delta T$. Some of the analysed standards give recommendations how the temperature
456 difference ΔT should be determined. According to CIRIA C766 [15] and ACI 207.2 [8] the temperature
457 drop should be calculated as the difference between the maximum (peak) temperature and ambient
458 temperature: $\Delta T = T_{\max} - T_a$. This means that the design thermal strain accounts for the whole
459 temperature drop during cooling. EN 1992-1-1:2023 [14], in turn, recommends that the thermal strain
460 responsible for cracking should be determined at the critical time t_{crit} which is the time instant when
461 cracking is likely to occur, and as a difference between the peak temperature and the temperature of the
462 restraining element at that time: $\Delta T = T_{\max} - T_0$. If no better data is available, the latter one can be
463 assumed as the ambient temperature, however, in the case of a wall-on-slab structure the actual
464 temperature of the restraining element (foundation) can be higher due to its re-heating by the hardening
465 wall. Furthermore, EN 1992-1-1:2023 accounts also for the fact that initial heating of the wall induces
466 positive compressive stresses which reduce the value of the proceeding tensile stresses during cooling.
467 Consequently, the standard recommends reducing the design thermal strain by the factor $k_T = 0.9$.
468 The above-mentioned provisions consider maximum mid-span, mid-section temperature, so the
469 maximum possible temperature in the whole wall over the whole period of concrete hardening. In case
470 of the elements with relatively low massivity, which are characterised by small variations of
471 temperature in the cross-section, this assumption is correct. The challenge arises in more massive
472 elements, such as the analysed wall, in which the cross-sectional temperature variation is non-
473 negligible. Given the risk of through cracking, confirmed in the observations of the actual wall, it may,
474 hence, seem reasonable to consider in the calculations the thermal strain which gives zero self-induced
475 stress (the strain on the so-called compensation line – see Fig. 6). CIRIA C766 [15] recommends in
476 such a situation to use the mean temperature in the cross-section which – assuming parabolic
477 distribution of temperature in the cross-section – can be calculated as $T_{\text{mean}} = T_{\text{int}} - \frac{1}{3}(T_{\text{int}} - T_{\text{sur}})$.
478 Given the above considerations, the input data taken for further calculations were collectively presented
479 in Table 5. When analysing the diagram of temperature development in the wall (Fig. A.4) it can be
480 seen that over the period when measurements were recorded – until the time of formwork removal – no

481 temperature equalisation was reached while the wall had already cracked. The exact time of cracking
 482 is, however, not known. Therefore, following the recommendations of CIRIA C766, the analysis was
 483 performed at the time t_{crit} of 3 days.

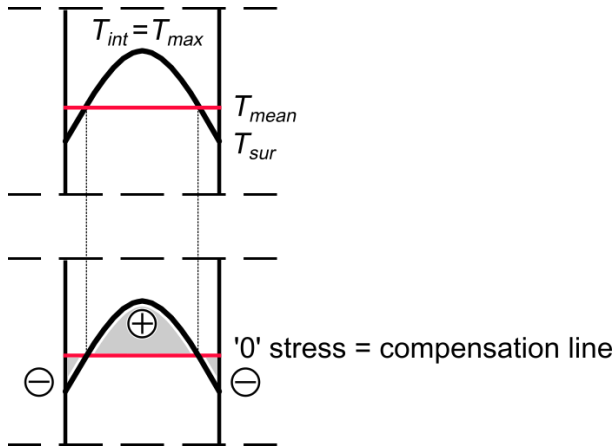


Figure 6. Method for determination of temperature for calculation of design early-age thermal strain.

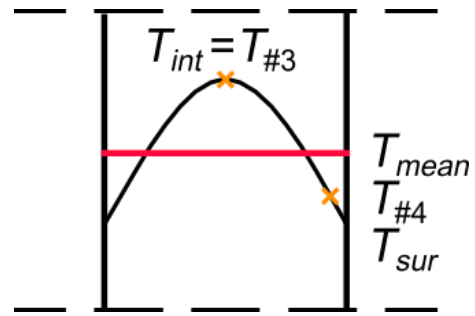


Figure 7. Mean temperature in the Civaux mock-up wall.

484 The temperature difference was calculated as the difference between the mean temperature in the cross
 485 section at the time of the peak temperature occurrence and the temperature of the foundation at t_{crit} .
 486 The peak temperature was the maximum temperature measured by thermocouple #3 located in the core
 487 of the wall while the surface temperature was calculated based on the measurements of thermocouples
 488 #3 and #4 (see Fig. 7). Temperature difference in the cross-section was equal to $\sim 9^{\circ}\text{C}$. The T_0
 489 temperature was taken from the measurements of thermocouple #1, which was located in the raft
 490 foundation just below the wall (see Fig. A.3). It can be observed that after re-heating to the temperature
 491 of $\sim 24^{\circ}\text{C}$, the raft cooled down steadily and after 5 days (up to when the measurements were available)
 492 it reached 20°C ; after 3 days its temperature was still around the peak value of 24°C (see Fig. A.4).

493 **Table 5.** Calculation of thermal strain 3 days after casting of the first lift in the Civaux mock-up wall.

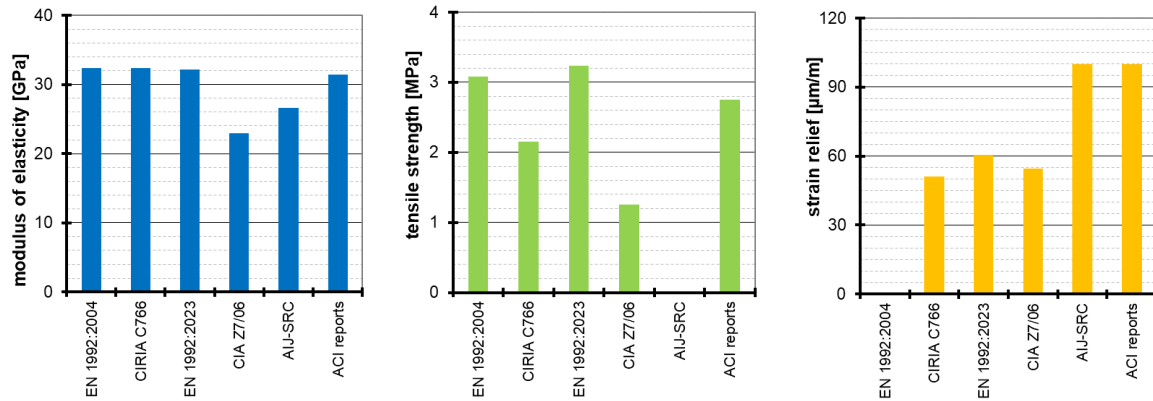
T_{max} [$^{\circ}\text{C}$]	59.3
T_{sur} [$^{\circ}\text{C}$]	50.2
T_{mean} [$^{\circ}\text{C}$]	56.3
T_a [$^{\circ}\text{C}$] – mean	11.4
T_0 [$^{\circ}\text{C}$]	24

$\Delta T = T_{\text{mean}} - T_0$ [°C]	32.3
$\varepsilon_T = \alpha_T \cdot (T_{\text{mean}} - T_0)$	323 $\mu\varepsilon$

494 It should be mentioned that time-development of concrete's properties is related to the progress of its
495 maturity, which is a temperature-dependent phenomenon. In case of massive structures, such as the
496 analysed wall, in which significant increase of temperature is observed over long period, these processes
497 develop visibly faster. Therefore, the equivalent age of concrete, not the real one, should be used for
498 determination of these values at the time of analysis. Normally, determination of the equivalent age is
499 difficult at the design stage when temperature history is not known. However, for the specific case of
500 the Civaux wall, the equivalent age of concrete, calculated according to EN 1992-1-1:2004 [5], at the
501 age of 3 days was approximately 10 days (calculated based on the mean temperature in the cross-
502 section), which is an important difference.

503 The value of the autogenous shrinkage strain was calculated using the laboratory test results presented
504 in Fig. A.5 with the EN 1992-1-1:2004 [5] model and least-square method approximation. At the time
505 $t_{\text{crit},eq} = 10$ days the autogenous shrinkage was estimated to be 30.3 $\mu\varepsilon$.

506 The compressive strength and modulus of elasticity were measured only since the 28th day. For early-
507 age analysis the measured 28th-day values were taken as a basis and the values of tensile strength and
508 modulus of elasticity at time $t_{\text{crit},eq}$ were calculated following each considered method. Figure 8
509 presents a comparison between the values obtained with these methods. It must be emphasised that the
510 CIA Z7/06 recommends fixed values of early-age tensile strength and modulus of elasticity for a 3-day
511 old concrete, which is a sensible value as long as the actual age and equivalent of this concrete comply.
512 For a massive structure such as the analysed one these recommendations are not valid.



513

514 **Figure 8.** Mechanical properties of the Civaux wall concrete after 3 days (10 days of equivalent age) assessed
 515 with different design methods.

516 Finally, to calculate the crack-inducing strain, the restrained part of imposed strain must be determined,
 517 which deems to know the degree of restraint (expressed with the restraint factor). Regarding the restraint
 518 factor, EN 1992-3 [6] recommends the maximum, default base restraint factor of 0.5 (which accounts
 519 for creep) while CIRIA C766 [15] recommends the default value of 0.8 (without considering creep).
 520 Alternatively, CIRIA C766 refers to the formula proposed by ACI 207.2 [8] given by Eq. (3), which
 521 according to Eq. (4) depends on the L/H ratio of the restrained element, and for the Civaux wall with
 522 $L/H \geq 10$ it is constant over the height. The relative stiffness of the wall depends, in turn, on the
 523 geometry of the wall and foundation A_c/A_F , which stay unchanged over the analysed period, and their
 524 moduli of elasticity E_c/E_F , which evolve in time. The restraint in this case is not typical, as it is in a
 525 form of a raft foundation. Following the recommendations of ACI 207.2 [8] in such a case it can be
 526 assumed that $A_c/A_F = 2.5$. The resultant restraint factor depends therefore on the applied time-
 527 development function of the modulus of elasticity which determines the E_c/E_F ratio, and differs among
 528 the methods only slightly from 0.72 to 0.73 (in elastic analysis). Finally, the restraint factor estimated
 529 with CIA Z7 [16] method in elastic analysis is equal to 0.82 (see Table 6), but it should be noted that
 530 CIA Z7 assumes the slowest development of the modulus of elasticity of all the methods (see Fig. 8b).
 531 Given the above, the restraint factor $R = 0.8$ was assumed for calculations as a safe estimate in all the
 532 methods where no specific recommendations were given. The effect of creep on partial relief of
 533 restrained strains was accounted for by reducing the value of the degree of restraint by factor $K_c =$

534 $1/(1 + \varphi)$ equal to 0.65 following CIRIA C766. The resultant restrained part of strain and crack-
 535 inducing strains are collectively presented in Table 6.

536 **Table 6.** Calculation of crack-inducing strain 3 days after casting of the first lift in the Civaux mock-up wall.

	EN 1992-1-1 :2004 & 1992-3:2006	CIRIA C766	EN 1992-1- 1:2023	CIA Z7/06	AIJ-SRC	ACI 207.2
Thermal strain ε_T	323 (from Table 5)					
Autogenous strain ε_{ca}	30.3					
Imposed strain ε_{imp}	353.3					
Restraint factor R	0.5 (creep)	0.8 (no creep) $K_c = 0.65$	0.5 (creep)	0.82 (no creep)	0.8 (no creep) $K_c = 0.65$	0.8 (no creep)
Restrained strain ε_{rest}	176.6	183.7	176.6	288.3	n/a	282.6
Crack-inducing strain $\varepsilon_{cr} =$ $\varepsilon_{rest} - k_t \varepsilon_{rctu}$	176.6	132.5	116.2	233.8	n/a	182.6

537 Table 6 collects also the predictions of the crack-inducing strain in the analysed wall calculated with
 538 different methods. The same value of the total free strain was assumed. The differences in the restrained
 539 strain result mainly from the differences in the assumed value of the restraint factor, while in the case
 540 of the crack-inducing strain further from the difference in the magnitude of the assumed strain relief
 541 (extensibility). Consequently, the lowest value of the crack-inducing strain is predicted with EN 1992-
 542 1-1:2023, then CIRIA C766 and EN 1992-1-1:2004 & EN 1992-3:2006, with comparable prediction of
 543 ACI 207.2 & 224, and the highest value is predicted with CIA Z7/06 method. This complies with the
 544 tendency defined in Table 4. No direct comparison can be made with the method of AIJ-SRC because
 545 of different assumptions of the model in which the crack-inducing strain is not explicitly calculated.

546 4.3 Crack width

547 The widths of the cracks predicted with the analysed methods differ significantly, with over triple
 548 difference between the extreme values (see Table 7).

549

550 **Table 7.** Calculation of crack width 3 days after casting of the first lift in the Civaux mock-up wall.

	EN 1992-1-1:2004 & EN 1992-3:2006	CIRIA C766	EN 1992-1-1:2003	CIA Z7/06	AIJ-SRC	ACI 207.2 & ACI 224	measured
Calculated slip length $2l_{e,max}$ [m]	0.75	1.00	0.60	1.00	$s_{r,max} = 2.17$ $s_0 = 0.17$	0.91	Max spacing 3.2
w_{max} [mm]	0.133	0.133	0.070	0.235	0.219	0.248	0.2 (0.5*)

* can possibly be treated as an exceptional anomaly

551 The methods of the current version of EN 1992-1-1:2004 & EN 1992-3:2006, CIRIA C766, EN 1992-
552 1-1:2023 and CIA Z7/06 are easily comparable because they are based on the same model. The
553 differences result first of all from the predicted transfer length over which the strain difference occurs.
554 It must be remembered that in case when the element is in the crack formation stage, the calculated
555 value of $s_{r,max}$ must be understood as twice the transfer length, and evidently all these methods predict
556 this distance to be significantly smaller than the crack spacing. The greatest length of strains
557 incompatibility is predicted with CIRIA C766 (and CIA Z7/06, which uses the same formula) because
558 of the assumption of poor bond properties. The smallest length is predicted with EN 1992-1-1:2023,
559 which in turn less conservatively takes into account the influence of both the bond properties and
560 concrete cover.

561 The differences in the crack width are further caused by the value of the restraint factor (hence the
562 restrained part of strain) and the level of strain relief. The highest magnitude of the crack-inducing strain
563 is predicted with CIA Z7/06 method in which the restrained strain is determined without taking into
564 account the effect of creep (linear-elastic restraint factor), which consequently results in the greatest
565 predicted crack width. EN 1992-1-1:2023, in turn, predicts the smallest magnitude of crack-inducing
566 strain, mainly due to the highest expected level of strain relief. This, coupled with small crack spacing,
567 results in the smallest predicted crack width. The methods of EN 1992-1-1:2004 and CIRIA C766 give
568 in this case comparable results.

569 Comparison of the remaining two methods (AIJ-SRC and ACI 207.2 & 224) is more difficult, because
570 they are based on different models. The same value of the restraint factor is taken in both methods. In

571 the AIJ-SRC approach the effect of creep is taken into account while in the ACI approach neglects the
572 effect of creep. Yet, the obtained width of the cracks are of comparable magnitude and are as large as
573 predicted by the CIA Z7/06 method.

574 Even though it is not an intention of the standardised methods to compare the calculated crack width
575 with those actually measured on site, it is a common practice to control the compliance of the structure
576 with its design by doing such comparison. This, however, requires understanding of the crack width
577 model assumptions. First of all, cracking is a highly stochastic process, and therefore some margin of
578 error must be accepted. This margin might be related to the difference between the calculated and
579 measured crack width, as discussed in [12]. Another point of view might be in the expected outcome.
580 For instance, if one takes into account possible uncontrollable random effects such as inaccuracies
581 during execution, it might be accepted that individual cracks might exceed the design limits as they can
582 be easily repaired with negligible effect on the integrity of the structure and the budget of the
583 investment.

584 Given the latter, i.e. if a single crack of 0.5 mm could be treated as an accepted, unique abnormality,
585 the crack widths predicted by the methods of CIA Z7/06, AIJ-SRC and ACI 207.2 & 224 (0.235, 0.219
586 and 0.248 mm – all greater than 0.2 mm) would be larger in comparison with the measured crack widths.
587 The methods of EN 1992-1-1:2004 & EN 1992-3:2006, CIRIA C766 and EN 1992-1-1:2023, however,
588 in this particular case underestimate the widths of the cracks to an unacceptable level. The characteristic
589 crack width is defined as the width with 5% probability of being exceeded, but even if the margin of
590 error of 20% would be assumed following *Beeby* [40], it would allow some cracks to reach up to 0.16
591 mm according to EN 1992-1-1:2004 & EN 1992-3:2006 and CIRIA C766, and even as little as 0.085
592 mm according to EN 1992-1-1:2023. With the maximum crack width of 0.2 mm the level of
593 underestimation is 50% for past EN 1992 and CIRIA C766, and almost 300% for new EN 1992-1-1.

594 **4.4 Minimum reinforcement**

595 A comment should be made on the applied reinforcement with respect to the minimum reinforcement
596 requirements. The applied reinforcement ($\phi 20$ cc 180 mm, $A_s = 17.5 \text{ cm}^2$) would be below the minimum
597 required reinforcement if one would take the tensile area of concrete right before cracking A_{ct} equal to
598 half the cross-section ($A_{s,\min} = 34.3 \text{ cm}^2$ in this case). While this is a good assumption for thin sections,

599 with increasing massivity of the element it becomes more and more incorrect, thus leading to
600 overestimation of the required reinforcement. In fact, the temperature variation in the cross-section,
601 which is responsible for the formation of self-induced stresses, leads to the fact the tensile stresses
602 develop only at some depth of the cross-section, while the interior of the wall is compressed (see Fig.
603 11). Localisation of the zero-stress (compensation) line is, however, extremally difficult to determine
604 at the design stage as it would require to simulate the thermal field in the wall.

605 Another important aspect is the model from which the formula for the minimum required reinforcement
606 was derived. The formula is based on the model of a tie, which does not represent the base-restrained
607 elements well. That is because in the base-restrained elements the strains are confined not only by
608 reinforcement, but also by the base, thus reducing the need for reinforcement. This fact is accounted for
609 by CIRIA C766 where a reduction coefficient k_{Edge} has been introduced to represent this confining
610 effect. The coefficient has been defined as $k_{\text{Edge}} = 1 - R_{\text{Edge}}$, where R_{Edge} is the degree of restraint
611 at the base. With the increasing restraint the value of the coefficient – and consequently the required
612 area of reinforcement – decrease.

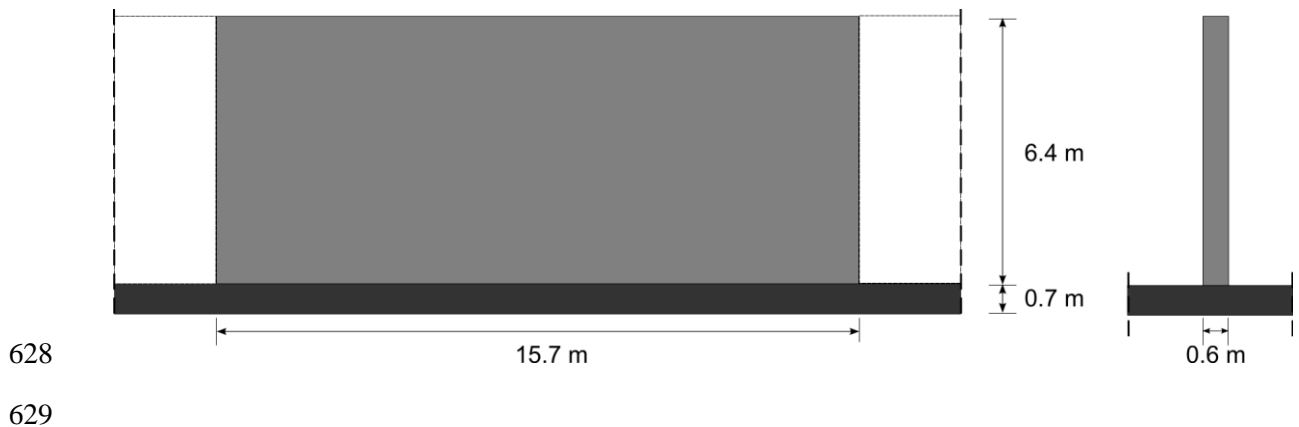
613 **5 Case study 2: heavily reinforced tank wall segment**

614 **5.1 Description of the structure**

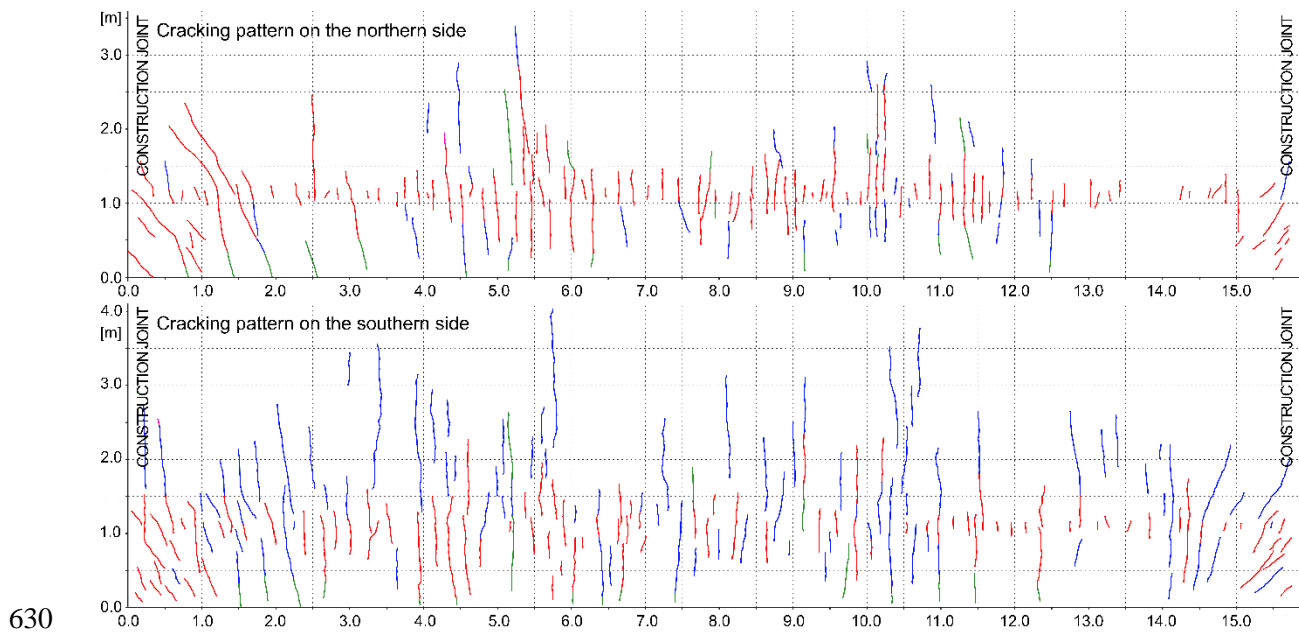
615 This case study was an internal segment of a wall in a rectangular reinforced concrete tank, restrained
616 along the base and along both vertical edges, classified as semi-massive according to [34]. Cracking of
617 the wall had been monitored for 9.5 months. Figure 9 schematically shows the geometry as well as
618 cracking pattern and its change in time in the wall. In the first stage, the width of the cracks did not
619 exceed 0.1 mm, they were mostly limited within a range of 0.025-0.05 mm, with individual cracks, not
620 in numbers that could present a risk for compromising the integrity of the structure, of 0.075 mm width.
621 At the second measurement stage, the measured crack widths only locally reached 0.15 mm, in other
622 cases they were limited to 0.1 mm. At the last measurement stage, the crack widths did not increase.

623 The data of the analysed case study including detailed description of the structure, its geometry,
624 manufacturing technology as well as the measurements of development of hydration heat and
625 mechanical properties, temperature development, shrinkage strains and creep under compression and

626 tension can be found in [41], [42], [43] and [44], while most important results are presented in the
627 Appendix, sec. A.2.



628
629

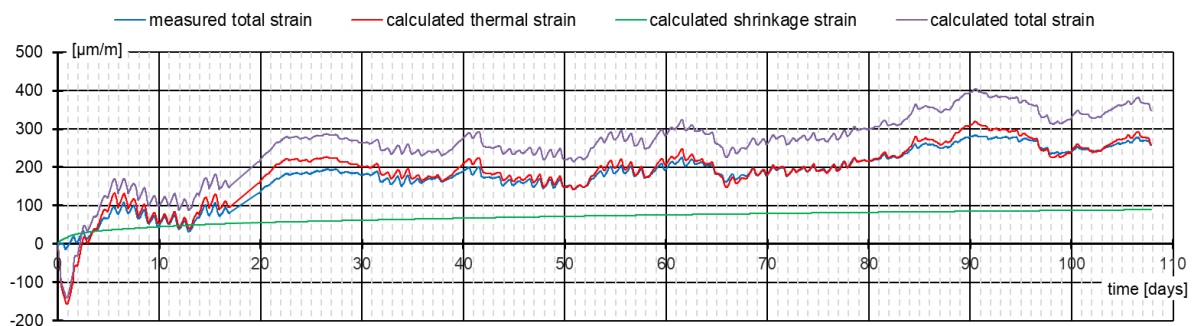


630
631 **Figure 9.** Tank wall segment: longitudinal view; cross-section; cracking pattern (16 days – red; 90 days – blue;
632 285 days – green).

633 5.2 Estimate of the early-age and long-term crack-inducing strain

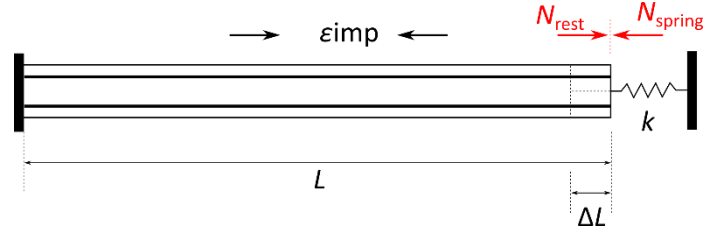
634 The main purpose of the analysis of this case study is to compare the predictions of crack spacing and
635 crack width change in time with developing strains using different methods. The calculations were
636 therefore performed at two time instants: at the age of 16 days (early-age) and 90 days (long-term). It
637 must be emphasised, however, that the first cracks appeared on the 2nd/4th day after casting while the
638 measurements of the cracks width and spacing were only made after 16 days.

639 The strains were calculated at the height of +1.40 m above the joint, at the level where crack widths
640 were measured. The temperature was taken as a mean temperature in the cross-section, determined from
641 the measurements in points B3 (core) and B4 (northern surface) (see Fig. A.8) because of a relatively
642 stable temperature distribution on that side of the wall. Drying shrinkage was also calculated as a mean
643 value in the cross-section. Figure 10 shows the diagrams of the total shrinkage strain, thermal strain,
644 autogenous shrinkage strain and drying shrinkage strain calculated in this point. Although at first glance
645 difference can be observed between the measured and calculated total strain, it must be explained that
646 the calculated thermal strain does not take into account the restraining effect, it is a theoretical strain in
647 a completely unrestrained element. The measured total strain, in turn, includes the restraining effect, so
648 the measured total strain represents only the unrestrained part of the sum of thermal and shrinkage
649 strains. Given the roughly estimated value of the restraint factor (calculated with Eq. (2)) of 0.2 it can
650 be demonstrated that the value of the restrained part of the total deformation is comparable to the
651 calculated free shrinkage. Consequently, the value of the free shrinkage strain used in calculations were
652 taken as $150 \mu\epsilon$ at 16 days and as $395 \mu\epsilon$ at 90 days.



654 **Figure 10.** Calculated free imposed strain at the level of + 1.40 m in the tank wall segment.

655 It is very relevant at this point to discuss the issue of the degree of restraint which is one of the decisive
656 factors in determination of the expected crack width (see Table 2). The width of the crack is expressed
657 as dependent on the restrained part of strain with the use of the restraint factor R . The standards do not,
658 however, differentiate the degree of restraint conditions before and after cracking – see e.g.
659 recommendations of EN 1992-1-1:2023 [14] in Annex D where the same restraint factor is used both
660 for the cracking risk assessment and the crack width.



661

662 **Figure 11.** Equilibrium of forces and compatibility of deformations in a partially restrained tie under imposed
 663 shrinkage strain (after [45]).

664 The restraint factor is defined on the basis of strains by Eq. (2) which can be expressed on the basis of
 665 deformations as:

$$666 \quad R = \frac{\varepsilon_{\text{imp}} \cdot L - \varepsilon_{\text{free}} \cdot L}{\varepsilon_{\text{imp}} \cdot L} = 1 - \frac{\Delta L}{\varepsilon_{\text{imp}} \cdot L} \quad (5)$$

667 where L is the length of the element and ΔL is its elongation due to imposed strain (see Fig. 1b). If the
 668 degree of external restraint is expressed with the stiffness of the spring k (Fig. 11), the conditions of
 669 equilibrium of forces $N_{\text{rest}} = N_{\text{spring}}$ and compatibility of deformations $\Delta L = \Delta L_{\text{spring}}$ can be defined.

670 With:

$$671 \quad \Delta L = \varepsilon_{\text{imp}} \cdot L + \frac{N_{\text{rest}}}{E_c(t) A_c (1 + \alpha_e \rho)} \cdot L \quad (6a)$$

$$672 \quad \Delta L_{\text{spring}} = \frac{N_{\text{spring}}}{k} \quad (6b)$$

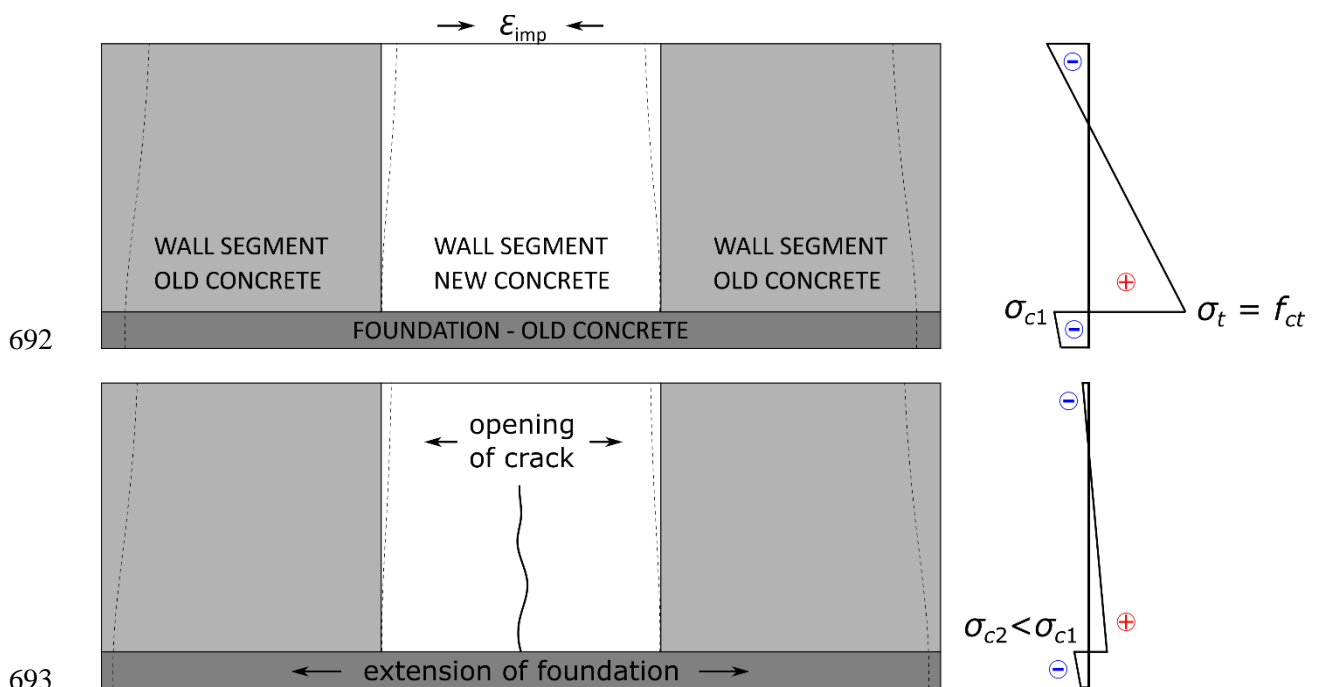
673 the degree of restraint can be expressed as:

$$674 \quad R = \frac{1}{1 + \frac{1}{k} \frac{E_c(t) \cdot A_c \cdot (1 + \alpha_e \rho)}{L}} \quad (7)$$

675 where $E_c(t) \cdot A_c \cdot (1 + \alpha_e \rho) / L$ is the axial stiffness of the element with respect to the included
 676 reinforcement. It can be noticed that in an uncracked element with the progressing time during
 677 hardening of concrete, due to the developing modulus of elasticity of concrete, the axial stiffness of the
 678 element will increase, thus the degree of restraint of the element decreases. However, once the cracking
 679 occurs, it will decrease the stiffness of the element, increasing the degree of restraint. This has been
 680 experimentally proven in [45].

681 When related to the actual case of a wall on foundation as the analysed case of a tank wall segment, the
 682 effect of increasing degree of restraint due to cracking can be illustrated with Fig. 12. Imposed
 683 deformations will cause tension over a certain height of the wall, and compression in the foundation,

684 which magnitude will increase with increasing imposed strains until tensile capacity of the wall is
 685 reached and a crack is formed. This will cause a relief of stresses immediately after cracking, both in
 686 the wall and in the foundation. This drop in the compressive stress in the foundation will lead to the
 687 extension of the foundation which, in turn, will cause additional opening of the crack, as a result of
 688 additional redistribution of imposed deformations. Therefore, if the width of the crack is to be calculated
 689 with the use of the approaches proposed in the standards, i.e. by applying the restraint factor for
 690 uncracked systems, then its magnitude in the cracked element must be higher than it would appear from
 691 the analysis of the uncracked element if the width of the crack is not to be underestimated.



692
 693
 694 **Figure 12.** Changes of deformation and stresses in a wall subjected to imposed shrinkage strain: (top) right before
 695 cracking; (b) right after formation of a crack and stress relief.

696 Nevertheless, exact calculation of the value of the restraint factor in the cracked elements is a
 697 challenging task which requires further studies and authors are not yet confident to provide here a
 698 quantitative recommendation. Therefore, for now, a conservative value of the restraint factor in an
 699 uncracked state of 0.8 was used for further calculations at all stages of the crack width control.

700 The input data for calculation of the expected crack spacing and crack width as well as their change in
 701 time are collectively presented in Table 8.

702

703 **Table 8.** Input data for calculations of crack widths and their change in time in a tank wall.

	16 days	90 days
Source of load	Hardening temperature Autogenous shrinkage	Autogenous shrinkage Drying shrinkage Ambient temperature fluctuations
Imposed strain ε_{imp} [$\mu\varepsilon$]	150	395
Restraint factor R	0.8	0.8
Effect of creep K	0.65	0.60
Modulus of elasticity E_{cm} [GPa]	18.8	22.0
Tensile strength f_{ctm} [MPa]	1.61	1.99

704 The crack-inducing strain was calculated from the restrained part of strain and strain relief as
 705 recommended by the methods. The calculated strains are collectively presented in Table 9.

706 **Table 9.** Crack-inducing strain [$\mu\varepsilon$] in a tank wall segment calculated with different standardised methods.

Strains [$\mu\varepsilon$]	Restrained strain		Tensile capacity		Crack-inducing strain	
	16 days	90 days	16 days	90 days	16 days	90 days
EN 1992-1-1:2004 & EN 1992-3:2006	78*	190*	86	91	78	190
CIRIA C766	78*	190*	92*	127*	32	126
EN 1992-1-1:2023	78*	190*	86	91	27	135
CIA Z7/06	120	316	86	91	34	225
AIJ-SRC	n/a*	n/a*	100***	150***	351****	480****
ACI 207.2 & 224	120	316	100***	150***	20	166

* considers the effect of creep on reduction of strain;

** considers sustained character of loading and effective modulus of elasticity

*** recommended fixed value

**** crack formation stage assumption

707 Large differences between the expected values of the crack-inducing strain can be observed, even
 708 though the same values of the imposed strain and restraint factor were assumed in all the methods (for
 709 basic assumptions of the methods refer to Table 2). This is related to the way in which each method
 710 takes into account the effect of creep on the restrained strain and how it predicts the level of strain relief
 711 after cracking. In EN 1992-3:2006 the restraint factor is reduced to consider creep but no strain relief is
 712 taken into account, thus the value of the crack-inducing strain is the highest. In case of CIRIA C766
 713 and EN 1992-1-1:2023, the level of extensibility is expected to be $0.5\varepsilon_{ctu}$ (46 and 63 $\mu\varepsilon$) and $0.6\varepsilon_{ctu}$

714 (51 and 54 $\mu\epsilon$), respectively, in addition to the same assumed reduction in the restraint factor, which
 715 explains lower values of crack-inducing strain. Finally, CIA Z7/06, AIJ-SRC and ACI 207.2 assume
 716 the level of extensibility at full ϵ_{ctu} . In case of CIA Z7/06 and ACI 207.2 no effect of creep is
 717 considered, so the methods predict by far the greatest values of the restrained strain but also the highest
 718 level of extensibility. As a results, the estimated values of the crack-inducing strain are in comparison
 719 moderate. Situation is different in case of the AIJ-SRC method which is based on the assumption of the
 720 crack formation phase. The crack-inducing strain, calculated considering creep, is much higher than
 721 predicted by other methods (even an order of magnitude at early age). However, its change in time is
 722 much less dramatic – the increase is by ~35% while for other methods the increase is from ~3 to even
 723 up to ~8 times.

724 5.3 Early-age and long-term crack width calculations

725 In the final step the crack spacing and crack width were calculated with the analysed methods with the
 726 focus on crack spacing and crack width change with the progressing increase of the imposed strains in
 727 time. The results of calculations are collected in Table 10.

728 **Table 10.** Early-age and long-term crack width in a tank wall segment.

	Crack spacing (mean) [cm]		Crack width (max) [mm]	
	16 days	90 days	16 days	90 days
measured	$s_{rm} = \sim 24$ cm	$s_{rm} = \sim 20$ cm	0.025–0.05, individual cracks 0.075	≤ 0.1 , individual cracks 0.15
EN 1992-1-1:2004 & EN 1992-3:2006	$s_{rm} = 17.6$ cm		0.023	0.057
CIRIA C766	$s_{rm} = 21.7$ cm		0.012	0.047
EN 1992-1-1:2023	$s_{rm} = 14.8$ cm		0.007	0.034
CIA Z7/06	$s_{rm} = 21.7$ cm		0.013	0.083
AIJ-SRC	$s_{rm} = 175.6$ cm	$s_{rm} = 36.7$ cm	0.057	0.078
ACI 207.2 & 224	$s_{rm} = 57.3$ cm	$s_{rm} = 11.3$ cm	0.019	0.032

729 It can be concluded that almost all the methods underestimated the crack widths to a probably
 730 problematic degree. Only the method of AIJ-SRC was somewhat closer to the measured value. With an
 731 accepted error of $\pm 20\%$ the predictions of this method would expect that majority of the cracks would

732 not exceed 0.057 mm and 0.078 mm, and would allow for the individual cracks of up to 0.068 mm after
733 16 days and 0.094 mm after 90 days, respectively.

734 The method of Eurocode 2 and all related to it, i.e. EN 1992-1-1:2004 & EN 1992-3:2006, CIRIA C766,
735 EN 1992-1-1:2023 and CIA Z7/06, are based on the simplifying assumption of the same bond strength
736 for the stabilised and the crack formation phase, and irrespectively of the level of imposed strain. This
737 means that regardless of the crack stage the same formula is used for calculation of the crack spacing /
738 transfer length ($s_{r,max} = 2l_{e,max}$). Hence, with the progressing imposed strain, the transfer length does
739 not change and the width of the crack increases proportionally to the increase of the strain. Both EN
740 1992-1-1:2004 and EN 1992-1-1:2023 predict twice the transfer length to be lower than the measured
741 crack spacing, especially EN 1992-1-1:2023, where the predicted spacing is 14.8 cm in relation to the
742 measured values of 24 and 20 cm (Table 10), which may indicate that the wall had still been in the
743 crack-formation stage. The low value of the transfer length might be one of the reasons for
744 underestimation of the crack width, especially at early age.

745 In that sense the philosophy of the models implemented in AIJ-SRC and ACI 207.2 guidelines better
746 reflects the actual behaviour of the wall where an increase in imposed strain caused not only widening
747 of the existing cracks, but also formation of new cracks. Consequently, over the analysed period
748 between 16th and 90th day the imposed strain increased over 2.5 times while the mean crack width only
749 doubled which was associated with a decrease of mean crack spacing by almost 20%. This effect is
750 observed in the predictions of both methods, however, in both cases the methods expect rather an
751 increase in the number of cracks than an increase in their width. According to AIJ-SRC the increase in
752 crack width is by 1.4 times while the decrease in spacing is by 5 times. In case of ACI 207 the increase
753 in crack width is by 1.6 times with also the 5-time decrease in spacing. Nevertheless, due to ~3 times
754 smaller crack spacings at both analysed time instants, the crack widths predicted by the ACI 207.2
755 method are ~3 times smaller than as per AIJ-SRC.

756 Another issue is that none of the crack models take into account larger shrinkage strains from drying
757 that occur at the surface of the element. These models only take into account the mean value, which for
758 the analysed wall may be several times smaller than the shrinkage at its surface. Thus, crack-inducing
759 strain in the locations of crack width measurements are underestimated in these models. Additionally,

760 the precise determination of the restraint factor after cracking remains an open issue [46]. Currently,
761 code models are based only on approximate values for an uncracked structure.

762 **6 Conclusions and future work**

763 The paper presents a critical analysis of the predictive capacity of standardised methods for crack width
764 control in edge-restrained reinforced concrete elements subjected to imposed strains. The study covered
765 relevant standardised methods implemented in the documents from Europe, Australia, Japan and the
766 USA. The predicted crack widths were compared for the three distinct case studies: a theoretical
767 demonstration example of a typical base-restrained wall, a massive wall on a raft foundation (Case
768 study 1) and a heavily-reinforced semi-massive tank wall segment with combined restraint conditions
769 (Case study 2). The study allowed to draw conclusions on the applicability of the methods for design
770 of various externally restrained elements for serviceability limit state of cracking.

771 All the analysed models for determination of the crack spacing are based on the model of a tie. This can
772 be a reasonable assumption to treat the element restrained along its edges as composed of the ‘slices’
773 behaving as ties, but only given that the actual degree of restraint is taken in calculations, not full
774 fixation at its extremities. This is done only in the methods implemented in AIJ-SRC recommendation
775 and ACI 207.2 report.

776 Furthermore, the cracking behaviour of the elements subjected to restrained imposed strains is governed
777 by the crack formation stage. The increase in the restrained strain results both in the increase of the
778 width of the existing cracks and formation of new cracks. The model for crack width control in such
779 elements must, therefore, correspond to the expected cracking stage, which – among the analysed
780 methods – is ensured only by the methods implemented in AIJ-SRC recommendation and ACI 207.2
781 report. The models proposed by EN 1992 standards family do not differentiate the length of the strains
782 incompatibility section in the vicinity of the crack for different cracking stages, hence indicating that
783 this length in the crack formation stage will be the same as in the stabilised cracking stage. It is known,
784 however, that the bond strength depends on the cracking stage and consequently, the slip length is
785 expected to be greater in the crack formation stage [47]. Therefore, the slip length calculated with the
786 formula proposed by EN 1992 in case of the restraint-induced cracking may often lead to

787 underestimation of the crack width. This approach might be, however, useful for the design of restrained
788 elements given that characteristics of these structures support the assumption of close-to-stabilised
789 crack spacing. This includes the maintaining of a high degree of restraint during crack formation and/or
790 high reinforcement ratio, as shown on the example of Case study 2. The expected final width of the
791 crack may be then sufficiently well assessed.

792 Nevertheless, the typical cracking patterns of edge-restrained elements are not well represented by the
793 assumption of the crack spacing in a stabilised crack pattern of a tie. As discussed in [48], the distance
794 between primary cracks in a wall on foundation orientates predominantly on geometrical conditions of
795 the element itself. Long walls are subject to through cracks over the entire wall with a crack distance of
796 1.2 times the wall height. Shorter walls, however, are rather subject to stopping cracks, whereby the
797 crack distance is in the range of 1.2 times the crack height. For through cracks over the entire height of
798 the wall the German Annex to EN 1992-1-1 [23] acknowledges this effect by proposing a crack distance
799 of 2 times the wall height on the safe side. Nevertheless, using such a geometrically derived crack
800 spacing in crack width calculations is only appropriate when applying deformation-compatible
801 approaches with sufficient regard of the formation of secondary cracks in the vicinity of primary cracks,
802 see e.g. [48].

803 Further, the transfer length is defined in relation to the ratio between the bar diameter and reinforcement
804 ratio. Effective reinforcement ratio should be used which is related to the effective tensile area of
805 concrete (actual zone of reinforcement impact). Some of the methods, e.g. AIJ-SRC, which are derived
806 for relatively thin elements disregard the fact the effective tensile area becomes smaller than the
807 concrete area with an increasing thickness of the wall, as shown on the example of Case study 1.
808 Moreover, the height of the effective tensile area (depth of the reinforcement impact zone) is not a
809 constant value dependent on the location of the reinforcement, but depends also on the thickness of the
810 cross-section, which is encountered by the German Annex to EN 1992-1-1 [23].

811 Even though the philosophy of the model is crucial for the design, proper choice of the input parameters
812 is of comparable importance. In both analysed case studies of real structures (Case 1 and 2) the
813 calculated widths of the cracks were underestimated, which may have a number of reasons in addition
814 to the underestimated crack spacing. First of all, the value of the imposed strain might be underestimated

815 by an assumption of a too low value of the coefficient of thermal expansion of concrete, which depends
816 strongly on the type of the aggregate used. The value of the shrinkage strain, especially drying shrinkage
817 strain, might be underestimated when mean value of shrinkage is taken in calculations while the
818 magnitude of drying near the surface can be significantly higher.

819 Secondly, the value of the restraint factor can be wrongly estimated. A challenge might lay in proper
820 assessment of the degree of restraint in non-standard restraining conditions, like the Case study 1 where
821 the restraining body was of a relatively low stiffness but had a form of a common foundation slab. In
822 semi-massive and massive walls which are most commonly subjected to imposed deformation, such as
823 those analysed in Case study 1 and 2, there is also a combined effect of external restraint and internal
824 restraint due to the strain variation in the cross-section. What is also not addressed by the analysed
825 methods is the fact that the degree of restraint in a cracked element is different than in an uncracked
826 element – it increases with the progressing cracking due to the reduction in stiffness of the element [45].
827 It is crucial to account for this fact in the design for crack control as the predicted width of the crack in
828 all the analysed methods depends directly on the assumed degree of restraint.

829 Finally, the value of the calculated crack-inducing strain depends on the level of the assumed
830 extensibility of concrete (ability of concrete to expand between the cracks) which is related to its tensile
831 capacity. The recommended value of the strain relief may vary from 0 (EN 1992-1-1:2004) to $100 \mu\epsilon$
832 at early age and $150 \mu\epsilon$ in long term (ACI 207.2). The examples of Case study 1 show that when the
833 design is performed based on the class of concrete, the extreme values of extensibility recommended
834 by ACI 207.2 are overestimated. This observation is further enforced in the example of Case study 2
835 which shows that other mechanical properties (tensile strength, modulus of elasticity, tensile capacity)
836 might be in reality lower than it would result from the predictions of the methods based on the
837 compressive strength. This is a common case when admixtures are added to the concrete mix to obtain
838 the required class. Therefore, a close cooperation between a designer and concrete technologist are
839 required already at the design stage as the example of Case study 2 demonstrates that the design of
840 special structures should not be based solely on the concrete class.

841 The above conclusions clearly show a need to develop a unified model for crack width control in edge-
842 restrained reinforced concrete elements subjected to imposed strains. The model must take into account

843 the nature of cracking in edge-restrained elements (especially the influence of geometrical conditions
844 on the distance between primary cracks and their growth over the wall), the actual stage of cracking and
845 slip between the reinforcing bars and concrete (slip-dependent bond law). In addition, it should be
846 generalised for various possible geometries and reinforcement, especially it should address the issues
847 inherent to massive elements, heavily-reinforced elements and elements with combined restraint
848 conditions. Furthermore, an agreement must be reached on the definition of the properties of concrete
849 which should be taken for the design, including mechanical properties of concrete and creep. Finally, it
850 is evident that a systematised study on the change of degree of restraint in walls during cracking is
851 needed. In addition to the above, the effect of combination of the external loads and imposed
852 deformations on prediction of the crack width is another complicated question that should be answered
853 in the future.

854 **Acknowledgements**

855 The authors would like to acknowledge the support of: Dirk Schlicke (TU Graz, Austria), Andy Gardner
856 (ARUP, Solihull, UK), Shingo Asamoto (Saitama University, Japan) and Tatsuya Usui (Taisei, Japan)
857 in preparation of the paper, as well as the financial support of Arup.

858 **Funding**

859 This work was supported by the Polish Ministry of Education and Science through the Silesian
860 University of Technology; FCT/MCTES through national funds (PIDDAC) under the R&D Unit
861 Institute for Sustainability and Innovation in Structural Engineering (ISISE) [UIDB/04029/2020]; the
862 Associate Laboratory Advanced Production and Intelligent Systems ARISE [LA/P/0112/2020].

863 **CRedit author statement**

864 **Agnieszka Jędrzejewska:** Conceptualization, Methodology, Formal Analysis, Investigation, Data
865 curation, Writing – Original draft, Visualisation, Project administration **Mariusz Zych:**
866 Conceptualization, Investigation, Resources, Writing – Review & Editing **Jean Michel Torrenti:**
867 Resources, Writing – Review & Editing **Fragkoulis Kanavaris:** Conceptualization, Writing – Review
868 & Editing, Funding acquisition **Miguel Azenha:** Conceptualization, Supervision, Writing – Review &
869 Editing **Fangjie Chen:** Resources **Shintaro Ito:** Resources.

870 **References**

- 871 [1] Jędrzejewska A, Kanavaris F, Zych M, Schlicke M, Azenha M. Experiences on early age thermal
872 cracking of wall-on-slab concrete structures. Struct 27: 2520-2549 (2020);
873 <https://doi.org/10.1016/j.istruc.2020.06.013>
- 874 [2] Fairbairn EMR, Azenha M, eds. Thermal cracking of massive concrete structures. State-of-the-art
875 Report of RILEM Technical Committee 254-CMS. Springer, Cham (2019);
876 <https://doi.org/10.1007/978-3-319-76617-1>
- 877 [3] Borosnyói A, Balazs GL. Models for flexural cracking in concrete: the state of the art. Struct
878 Concrete 6(2): 53-62 (2005); <https://doi.org/10.1680/stco.2005.6.2.53>
- 879 [4] Lapi M, Orlando M, Spinelli P. A review of literature and code formulations for cracking in R/C
880 members. Struct Concrete 19: 1481-1503 (2018); <https://doi.org/10.1002/suco.201700248>
- 881 [5] EN 1992-1-1:2004+A1:2014 – Eurocode 2. Design of concrete structures – Part 1-1: General rules
882 and rules for buildings (2014).
- 883 [6] EN 1992-3:2006 – Eurocode 2. Design of concrete structures – Part 3: Liquid retaining and
884 containing structures (2006).
- 885 [7] Bamforth PB. CIRIA C660: Early-age thermal crack control in concrete. CIRIA, London, UK
886 (2007)
- 887 [8] ACI 207.2R-07: Report on thermal and volume change effects on cracking of mass concrete
888 (2007).
- 889 [9] Guidelines for control of cracking of mass concrete 2016. Japan Concrete Institute, Technical
890 Committee on English version of JCI guidelines for control of cracking of mass concrete (2017).
- 891 [10] Klemczak B, Żmij A. Reliability of standard methods for evaluating the early-age cracking risk of
892 thermal-shrinkage origin in concrete walls. Constr Build Mater 226: 651-661 (2019);
893 <https://doi.org/10.1016/j.conbuildmat.2019.07.167>
- 894 [11] Zych M. History of the development of analytical models of cracking of restrained walls on a given
895 edge since 1968. Int J Concr Struct M 16 (2022); <https://doi.org/10.1186/s40069-022-00555-3>

- 896 [12] Jędrzejewska A, Zych M, Kanavaris F, Chen F, Ito S, Torrenti J-M, Schlicke D, Asamoto S,
897 Azenha M. Standardised models for cracking due to restraint of imposed strains – the state of the
898 art. *Struct Concrete* 24(4): 5388-5405 (2023); <https://doi.org/10.1002/suco.202200301>
- 899 [13] FprEN 1992-1-1:2022 [Final draft] – Eurocode 2: Design of concrete structures – Part 1-1: General
900 rules – Rules for buildings, bridges and civil engineering structures (Nov 2022)
- 901 [14] EN 1992-1-1:2023 – Eurocode 2: Design of concrete structures – Part 1-1: General rules – Rules
902 for buildings, bridges and civil engineering structures (Nov 2023).
- 903 [15] Bamforth P. CIRIA C766: Control of cracking caused by restrained deformation in concrete.
904 CIRIA, London, UK (2018)
- 905 [16] CIA Z7/06 – Concrete cracking and crack control, Concrete Institute of Australia (2017)
- 906 [17] Architectural Institute of Japan: Recommendations for practice of crack control in reinforced
907 concrete buildings (Design and construction), 2006. [in Japanese]
- 908 [18] ACI 224R-01: Control of cracking in concrete structures (2001, Reapproved 2008)
- 909 [19] ACI 207.2R-95: Effect of restraint, volume change and reinforcement on cracking of mass concrete
910 (1995; Reapproved 2005)
- 911 [20] El Khoury K, Ridley I, Vollum R, Forth J, Shehzad M, Elwakeel A, Nikitas N, Izzuddin B.
912 Experimental assessment of crack width estimations in international design codes for edge
913 restrained walls. *Structures* 55: 1447-1459 (2023); <https://doi.org/10.1016/j.istruc.2023.06.087>
- 914 [21] Klausen A. Early age crack assessment: codes, guidelines and calculation methods. DaCS Report
915 np. 02. SINTEF Building and Infrastructure, Trondheim, Norway (2018). Available online:
916 [https://www.sintef.no/contentassets/a2c5a98a03594086b7e6e872c02f39f7/dacs-report-no-2-](https://www.sintef.no/contentassets/a2c5a98a03594086b7e6e872c02f39f7/dacs-report-no-2-wp1.2-early-age-crack-assessment.pdf)
917 [wp1.2-early-age-crack-assessment.pdf](https://www.sintef.no/contentassets/a2c5a98a03594086b7e6e872c02f39f7/dacs-report-no-2-wp1.2-early-age-crack-assessment.pdf), last accessed on 18/08/2023
- 918 [22] CROW-CUR Report 1:2020 – Crack width control of concrete structures (2020) [unpublished]
- 919 [23] DIN EN 1992-1-1/NA:2013-04: National Annex to EN 1992-1-1: Design of concrete structures –
920 Part 1-1: General rules and rules for buildings (2013)
- 921 [24] Carino NJ, Clifton JR. Prediction of cracking in reinforced concrete structures. NISTIR 5634.
922 Building and Fire Research Laboratory, National Institute of Standards and Technology,

923 Gaithersburg, (1995). Available online:
924 <https://nvlpubs.nist.gov/nistpubs/Legacy/IR/nistir5634.pdf>, last accessed on 18/08/2023.

925 [25] Gilbert RI. Shrinkage cracking in fully restrained concrete members. ACI Struct J 89(2): 141–149
926 (1992); <https://doi.org/10.14359/2917>

927 [26] Base GD, Murray MH. Controlling shrinkage cracking in restrained reinforced concrete.
928 Proceedings of the 9th Australian Road Research Board (ARRB) Conference. Volume 9. Brisbane,
929 Australia: ARRB, p. 167–73 (1978)

930 [27] Schlicke D, Dorfmann EM, Fehling E, Tue NV. Calculation of maximum crack width for practical
931 design of reinforced concrete. Civil Engineering Design 3: 45–61 (2021)
932 <https://doi.org/10.1002/cend.202100004>

933 [28] Tan R, Hendriks M, Geiker M, Kanstad T. Analytical calculation model for predicting cracking
934 behavior of reinforced concrete ties. Journal of Structural Engineering (United States) 146(2):
935 04019206 (2020) [https://doi.org/10.1061/\(ASCE\)ST.1943-541X.0002510](https://doi.org/10.1061/(ASCE)ST.1943-541X.0002510)

936 [29] Somma G, Vit M, Frappa G, Pauletta M, Pitacco I, Russo G. A new cracking model for concrete
937 ties reinforced with bars having different diameters and bond laws. Engineering Structures 235:
938 112026 (2021) <https://doi.org/10.1016/j.engstruct.2021.112026>

939 [30] EN 206:2013+A2:2021 – Concrete – Specification, performance, production and conformity
940 (2021)

941 [31] ACI 209.2R-08: Guide for modeling and calculating shrinkage and creep in hardened concrete
942 (2008)

943 [32] Azenha M, Kanavaris F, Schlicke D, Jędrzejewska A, Benboudjema F, Honorio T, Šmilauer V,
944 Serra C, Forth J, Riding K, Khadka B, Sousa C, Briffaut M, Lacarrière L, Koenders E, Kanstad T,
945 Klausen A, Torrenti J-M, Fairbairn EMR. Recommendations of RILEM TC 287-CCS: thermo-
946 chemo-mechanical modelling of massive concrete structures towards cracking risk assessment.
947 Mat Struct 54: 135 (2021); <https://doi.org/10.1617/s11527-021-01732-8>

948 [33] Knoppik-Wróbel A, Klemczak B. Degree of restraint concept in analysis of early-age stresses in
949 concrete walls. Eng Struct 102: 369-386 (2015); <https://doi.org/10.1016/j.engstruct.2015.08.025>

- 950 [34] Kanavaris F, Jędrzejewska A, Sfikas IP, Schlicke D, Kuperman S, Šmilauer V, Honório T,
951 Fairbairn EMR, Valentim G, Funchal de Faria E, Azenha M. Enhanced massivity index based on
952 evidence from case studies: Towards a robust predesign assessment of early-age thermal cracking
953 risk and practical recommendations. *Const Build Mater* 271: 121570 (2021);
954 <https://doi.org/10.1016/j.conbuildmat.2020.121570>
- 955 [35] *fib* Bulletin 13: Nuclear containments (2001)
- 956 [36] Benboudjema F, Torrenti JM. Early-age behavior of concrete nuclear containments. *Nucl Eng Des*
957 238(10):2495-2506 (2008); <https://doi.org/10.1016/j.nucengdes.2008.04.009>
- 958 [37] Granger L. Comportement différé du béton dans les enceintes de centrales nucléaires: analyse et
959 modélisation. PhD Thesis, Ecole Nationale des Ponts et Chaussées, France (1995) [in French]
- 960 [38] Ithurralde G, de Larrard F, Nectoux J: Bétons à hautes performances (BHP) pour l'étanchéité des
961 structures en béton. Expérimentation. *Annales de l'Institut technique du bâtiment et des travaux*
962 *publics* 502:77-115 (1992)
- 963 [39] Buffo-Lacarrière L, Sellier A, Turatsinze A, Escadeillas G. Finite element modelling of hardening
964 concrete: application to the prediction of early age cracking for massive reinforced structures.
965 *Mater Struct* 44:1821-1835 (2011); <https://doi.org/10.1617/s11527-011-9740-y>
- 966 [40] Beeby AW. Fixing in cracked concrete – The probability of coincident occurrence and likely crack
967 width. CIRIA, London, UK (1990)
- 968 [41] Seruga A, Zych M. Research on thermal cracking of a rectangular RC tank wall under construction.
969 I: Case study. *J Perform Constr Fac* 30(1): 04014198 (2016);
970 [https://doi.org/10.1061/\(ASCE\)CF.1943-5509.0000704](https://doi.org/10.1061/(ASCE)CF.1943-5509.0000704)
- 971 [42] Zych M. Case study of concrete mechanical properties development based on heat temperature
972 measurements. *Cement Lime Concrete* 20(6): 383-392 (2015).
- 973 [43] Zych M, Seruga A. A new model for crack control in reinforced concrete tank walls. Part II:
974 Comparison with experimental results. *ACI Struct J* 116(3): 95-105 (2019);
975 <https://doi.org/10.14359/51713317>
- 976 [44] Seruga A, Zych M. Research of concrete creep at early age under compressive and tensile stresses.
977 *Cement Lime Concrete* 21(2): 65-77 (2016).

- 978 [45] Schlicke D, Hofer K, Tue NV. Adjustable restraining frames for systematic investigation of
979 cracking risk and crack formation in reinforced concrete under restrained conditions. In: M. Serdar
980 et al. (eds.), *Advanced Techniques for Testing of Cement-Based Materials*, Springer Tracts in Civil
981 Engineering. Springer, Cham, pp. 211-239 (2020); https://doi.org/10.1007/978-3-030-39738-8_7
- 982 [46] Zych M. The effect of the degree of cracking on the state of stress and cracks width in elements
983 with restrained boundary conditions. *Structural Concrete* 24(6): 7091–7102 (2023);
984 <https://doi.org/10.1002/suco.202300362>
- 985 [47] *fib Model Code 2010*, 2013
- 986 [48] Schlicke D. Mindestbewehrung zwangbeanspruchter Betonbauteile unter Berücksichtigung der
987 erhärtungsbedingten Spannungsgeschichte und der Bauteilgeometrie. PhD Thesis, Graz University
988 of Technology, Graz, Austria (2014) [in German]

989 **APPENDIX: Detailed descriptions of Case studies**

990 **A.1 Case study 1: Massive wall of Civaux NPP mock-up**

991 The analysed wall was an experimental mock-up nuclear containment wall tested by EDF in early 1980s
 992 within the THM (thermo–hydro–mechanical) task of the CEOS.fr project related to safety analysis of a
 993 newly constructed nuclear power plant near Civaux, France. The wall was 1.2 m thick, 2.8 m high (in
 994 total, divided into two lifts of 1.9 m and 0.9 m) and 20 m long, supported on a 0.4 m-thick raft foundation
 995 (see Fig. A.1). Breaks between the execution of the following segments were ~2 weeks. The main
 996 reinforcement of the wall was $\varnothing 20$ bars spaced vertically by 200 mm and horizontally by 180 cm (steel
 997 strength $f_{yk} = 400\text{MPa}$ and modulus of elasticity $E_s = 203\text{ GPa}$ with 5 cm concrete cover – see Fig. A.2).
 998 Vertical tubes for prestressing were also installed at the depth of 50 cm, spaced at ~80 cm. The wall
 999 was made with OPC concrete whose details of mix composition and resulting properties are enlisted in
 1000 Table A.1.



1001
1002 **Figure A.1.** Geometry of the Civaux mock-up wall: (a) longitudinal view; (b) cross-section.

1003 **Table A.1.** Composition and mechanical properties of concrete used for a Civaux mock-up wall [35].

Composition [kg/m ³]		Characteristics and results	
Aggregate	1872	Density [t/m ³]	2.33
Filler (limestone)	0	28-day compressive strength [MPa]	40.2
Silica fume	0	28-day tensile strength [MPa]	3.7
Cement CEM II/A 42.5R	350	28-day modulus of elasticity [GPa]	33.7
Water	195	Coefficient of thermal dilation [1/°C]	10×10 ⁻⁶
Superplasticiser	1		

1004 The wall was equipped with thermocouples to follow the evolution of the temperature in different
 1005 locations – Figure A.3 shows the locations of thermocouples while Figure A.4 shows the diagrams of
 1006 temperature development in chosen points in the wall (valid measurements only). The initial

1007 temperature of concrete of the wall was 19°C while the temperature of the foundation, which had
 1008 already been hardened and pre-cooled to the temperature of the environment at the moment when the
 1009 wall was cast, was 7°C. The formwork was removed after 5 days and at that moment the measurements
 1010 stopped. The wall heated up to the maximum of almost 60°C and the difference between the core and
 1011 near-surface temperature was ~6°C.

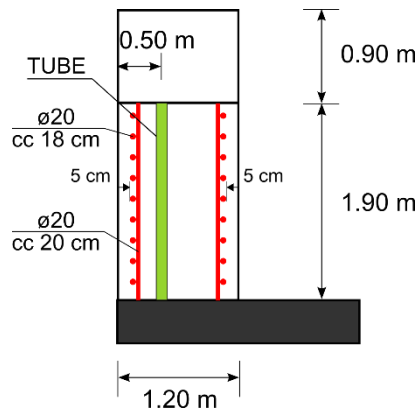


Figure A.2. Details of reinforcement in the Civaux mock-up wall (lift 1 only).

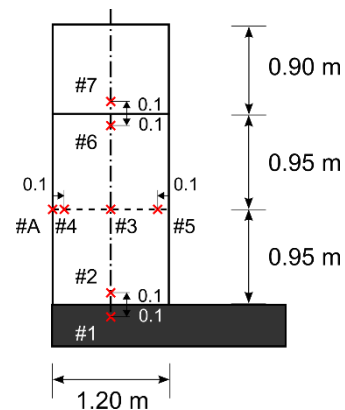


Figure A.3. Locations of thermocouples in the Civaux mock-up wall.

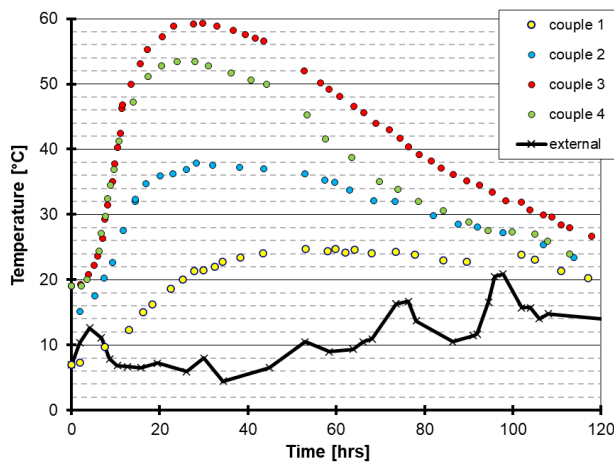


Figure A.4. Temperature development in the Civaux mock-up wall [36].

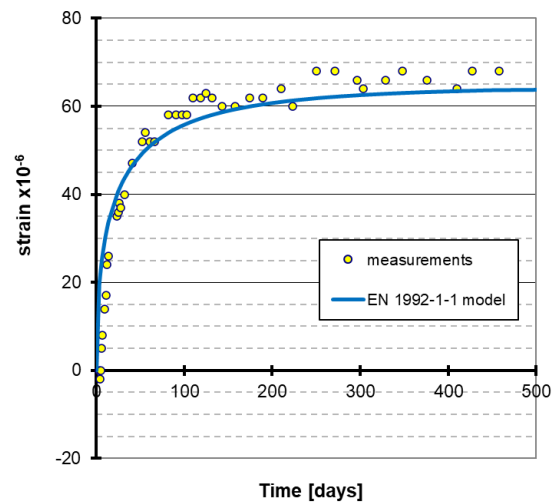


Figure A.5. Autogenous shrinkage strains of concrete used in the Civaux mock-up wall [37].

1012 The measurement of autogenous shrinkage was performed independently in the laboratory on the exact
 1013 same concrete mix as used for the construction of the wall. The tests were carried out on the cylindrical
 1014 samples of $\phi 16$ cm diameter and 1 m length, and the measurements were made in the central part of the

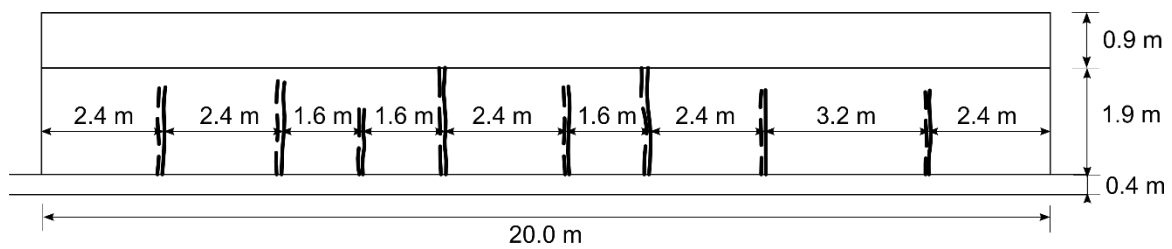
1015 sample. Figure A.5 presents the results of the measurement of autogenous shrinkage strains. The
 1016 measurements were approximated with the function proposed by EN 1992-1-1:2004 [5] as:

$$1017 \quad \varepsilon_{ca}(t) = [1 - \exp(-0.2 \cdot t^{0.5})] \cdot \varepsilon_{ca,\infty} \quad (A.1)$$

1018 where the final value of the autogenous shrinkage was determined to be $\varepsilon_{ca,\infty} = 64.6 \mu\varepsilon$.

1019 Drying shrinkage was not taken into account because cracking was formed before drying began (before
 1020 removing the formwork).

1021 Figure A.6 shows the cracking pattern in a Civaux mock-up wall. 8 cracks were formed which location
 1022 at both surfaces of the wall indicated that the cracks were through. The cracks were in general spaced
 1023 by 1.6 / 2.4 / 3.2 m, which corresponds to 2×, 3× and 4× the spacing of the vertical tubes for prestressing.
 1024 The widths of the cracks were 1 × 0.04 mm, 4 × 0.1 mm, 2 × 0.2 mm and 1 × 0.5 mm. Unfortunately,
 1025 it has not been specified what was the exact width of particular cracks and which crack had an excessive
 1026 width of 0.5 mm.



1027

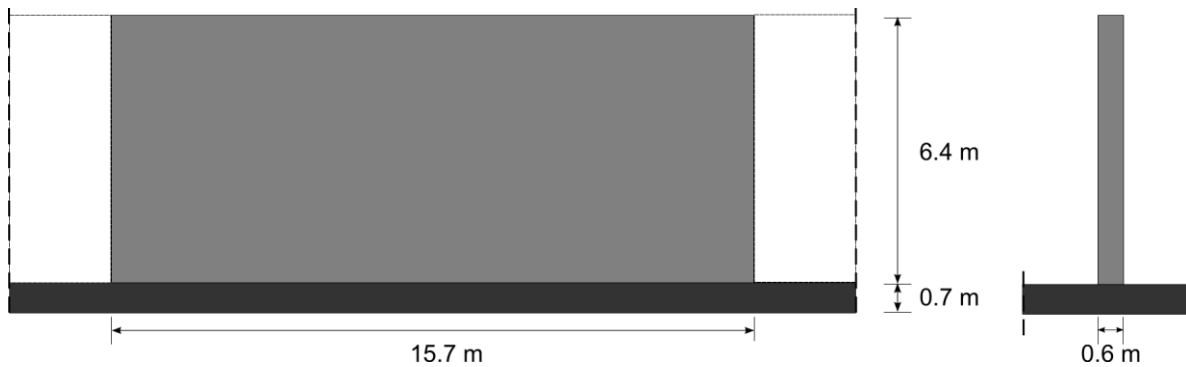
1028 **Figure A.6.** Cracking pattern in the Civaux mock-up wall [36][38].

1029 The *a posteriori* numerical analyses of the wall [36] [39] confirmed the observed cracking pattern and
 1030 that the cracks were through cracks. According to the results of these simulations, due to the fact that
 1031 the wall was kept in the formwork over the cooling phase, higher tensile stresses developed in the
 1032 interior of the wall where crack formation initiated in the core of the wall, additionally aided by
 1033 weakening of the cross-section by the location of the vertical tubes (“grooves”). Soon after, cracking
 1034 penetrated towards the surfaces of the wall. Even though the effect of external restraint could be regarded
 1035 as weak because of a relatively low thickness of the foundation with respect to the wall, it must be
 1036 remembered that the wall was cast on a common raft plate. As a consequence, the external restraint was
 1037 responsible for the fact that the formed cracks reached the joint while the length-to-height ratio > 10 led
 1038 to the cracks developing significant heights (> 80% height of the wall) with some cracks over the whole
 1039 height of the lift.

1040 **A.2 Case study 2: heavily reinforced tank wall segment**

1041 This case study is an internal segment of a semi-massive wall in a rectangular reinforced concrete tank,
1042 restrained along the base by a foundation slab and along both vertical edges by previously executed
1043 wall segments. Cracking of the wall had been monitored for 9.5 months. During this period, both early-
1044 age and long-time strains occurred, which were related to concrete shrinkage and changes in ambient
1045 temperature in the winter.

1046 The discussed tank with horizontal dimensions of 96.90×50.40 m and a wall height of 6.9 m was
1047 executed without expansion joints. The length of the analysed segment was 15.7 m and its height
1048 without slants and the crowning beam was 6.4 m (Fig. A.7). The wall had a thickness of 60 cm.



1049

1050 **Figure A.7.** Geometry of the tank wall segment: (a) longitudinal view; (b) cross-section.

1051 The composition of the concrete mix for the execution of C30/37 class concrete is shown in Table A.2.
1052 Tests results of compressive strength, tensile strength and modulus of elasticity of concrete are
1053 summarised in Table A.3. It should be emphasised that the concrete mix was designed to satisfy the
1054 requirements of the class, hence the 28-day compressive strength reached 32 MPa, but the value of the
1055 mean modulus of elasticity and mean tensile strength measured for this concrete were lower than one
1056 would predict with e.g. EN 1992-1-1:2004.

1057 **Table A.2.** Composition of concrete mix used in construction of the tank [41].

Concrete mix component	Content [kg/m ³]
Cement CEM III/A 32.5N (36-65% GGBFS)	380
Gravel 8/16	641
Gravel 2/8	439
Sand 0/2	619

Water	175
FM 21	4.56
LP 70	0.87
Air content [%]	4.5

1058 **Table A.3.** Mechanical properties of concrete used in construction of the tank [41].

Concrete age [days]	1	1.5	2	3	4	5	7	14	28	60	90
f_{ck} [MPa]	3.3	---	6.13	8.18	9.73	11.54	15.32	23.7	32	---	---
E_{cm} [GPa]	6.9	---	11.25	12.25	13.6	14.7	16.55	18.65	20.55	---	22
f_{ctm} [MPa]	---	0.74	0.92	---	1.1	1.26	1.44	---	1.71	1.84	1.99

1059 In order to be able to determine the values of the mechanical properties at various time instants, the
1060 results of measurements were represented with the time development function:

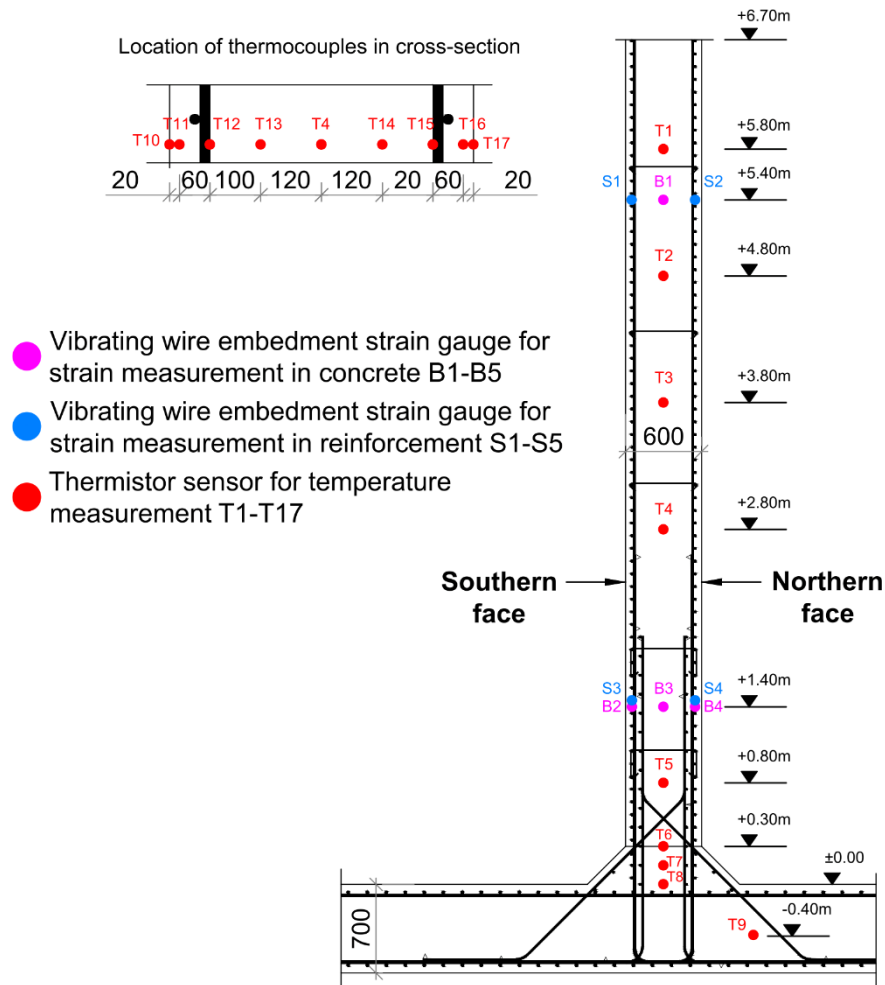
$$1061 \quad f_i(t) = \left[\exp \left[s_i \cdot \left(1 - \sqrt{\frac{28}{t}} \right) \right] \right]^{n_i} \cdot f_i(28) \quad (\text{A.2})$$

1062 where f_i is the mechanical property of concrete: tensile strength, modulus of elasticity and tensile
1063 capacity, respectively. This formula was adopted from EN 1992-1-1. In Eq. (A.2) $f_i(28)$ is the value of
1064 the given property at the age of 28 days, while coefficients s_i and n_i allow to calibrate the rate of
1065 development of each property. The values of relevant parameters in Eq. (A.2) determined using the
1066 least square approximation are collectively presented in Table A.4.

1067 **Table A.4.** Parameters of the time-development function of mechanical properties of the tank wall concrete.

Modulus of elasticity			Tensile strength		
$E_c(28)$ [GPa]	s_E	n_E	$f_t(28)$ [MPa]	s_f	n_f
20.65	0.67	0.36	1.74	0.61	0.40

1068 The layout of the reinforcement in the wall is illustrated in Fig. A.8. The steel of A-III/RB400W class
1069 was used ($f_{yk} = 350$ MPa). Up to the height of 2.0 m the wall was reinforced in two layers, i.e. $\phi 20$ every
1070 100 mm and $\phi 20$ every 150 mm ($\rho = 1.74\%$). Above 2.0 m, the reinforcement was placed in one layer,
1071 i.e. $\phi 20$ every 100 mm ($\rho = 1.05\%$). Concrete cover was 40 mm.

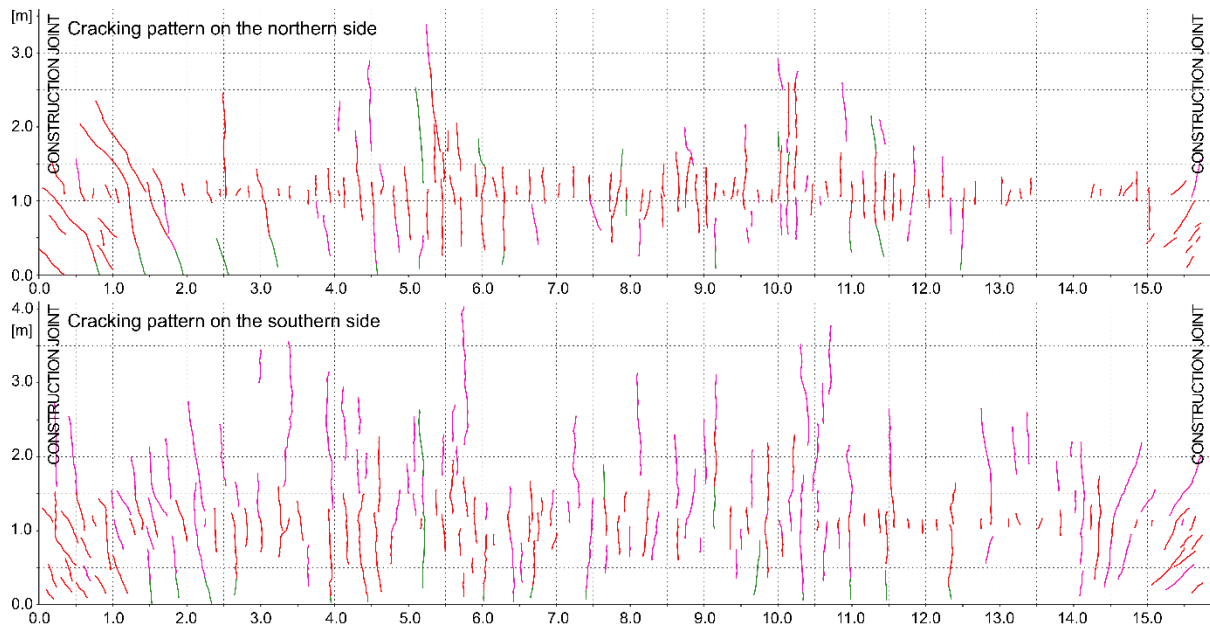


1072

1073 **Figure A.8.** Reinforcement layout and arrangement of measuring sensors in the tank wall segment.

1074 The analysed segment was concreted in summer. The formwork on the southern wall surface was
 1075 removed after 20 hours while on the northern surface after 40 hours. Measurements of strains with
 1076 Demec strain gauge were carried out after the formwork had been removed from the wall along its entire
 1077 length at a height of 1.1 m above the upper surface of the slant (level + 1.40 m).

1078 Figure A.9 illustrates the cracking pattern and its development from 16 days, through 90 days up to 285
 1079 days. First cracks appeared 2 days and 4 days after casting of the tank wall segment on the southern and
 1080 northern side, respectively. It was characteristic that the first cracks occurred in large numbers, but their
 1081 lengths and widths were very limited (0.025 to 0.075 mm). The reason behind this was partly the high
 1082 ratio of wall reinforcement ($\rho = 1.74\%$) and a significant contribution of self-equilibrating stresses. The
 1083 difference in the crack formation process on the northern and southern surfaces resulted from different
 1084 time of removing the formwork from both surfaces. It was found that in this first stage of measurements
 1085 (i.e. after 16 days), the widths of the cracks did not exceed 0.1 mm.



1086

1087 **Figure A.9.** Stages of cracking of the tank wall segment: a) northern surface, b) southern surface.

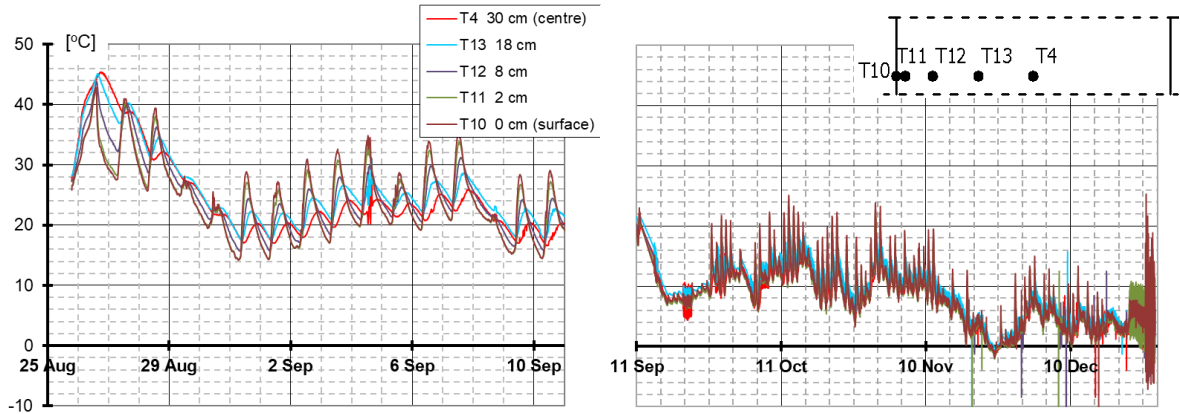
1088 (16 days – red; 90 days – pink; 285 days – green).

1089 Comparing the change in the crack layout in the period from the 16th day after concreting to the crack
 1090 layout after 3 months (see Fig. A.9), i.e. the period in which only additional imposed strains occurred,
 1091 a significant increase in the number of cracks and their length up to 4.0 m on both surfaces was
 1092 noticeable. During this period, the average crack spacing was reduced from 0.24 m to 0.20 m, the crack
 1093 widths locally reached 0.15 mm, and in other cases they would be limited to 0.1 mm.

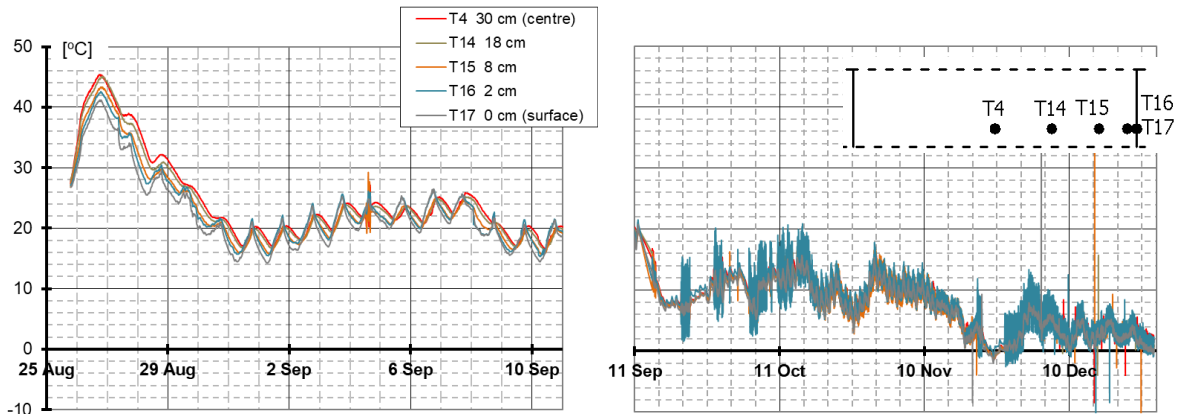
1094 The final stage of crack formation was surveyed after 9.5 months. This stage included the water-
 1095 tightness test of the tank and further imposed strains. Comparing this period with the period of 3 months,
 1096 a small number of new cracks and the elongation of a few cracks towards the lower edge of the wall
 1097 were observed. In this last stage of the measurements the crack widths did not increase. 9.5 months after
 1098 concreting the wall at the level of 1.1 m the measured mean crack spacing was 0.174 m on the northern
 1099 surface of the wall and 0.187 m on the southern surface. Only on the southern surface, the average crack
 1100 width was locally exceeding 0.1 mm.

1101 The temperature was measured in several points on the wall located both along its height and its
 1102 thickness (see Fig. A.8). The measured temperature changes and distribution in the period of concrete
 1103 hardening and over the period of 4 months are presented in Fig. A.10 and Fig. A.11.

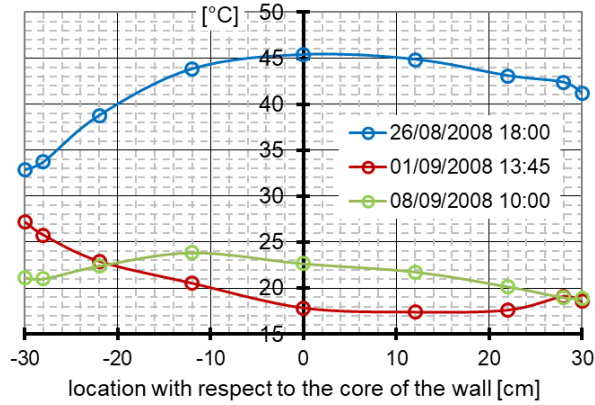
1104



1105



1106



1107

Figure A.10. Temperature measured at the thickness of the wall and its change in time

1108

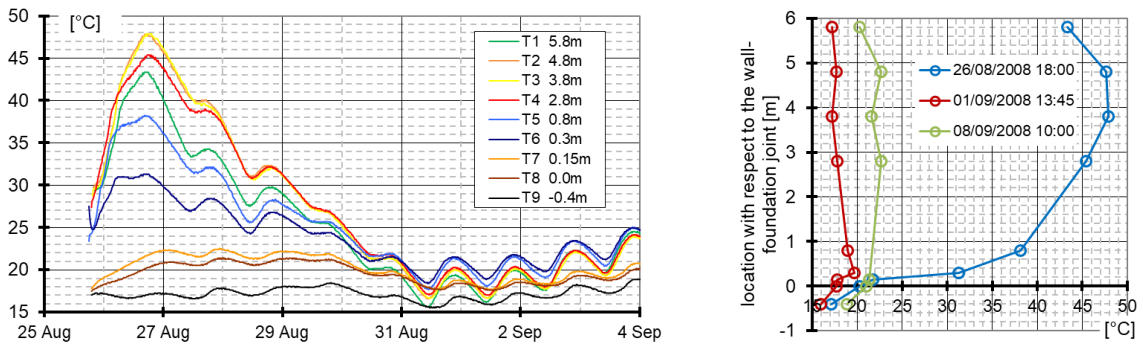
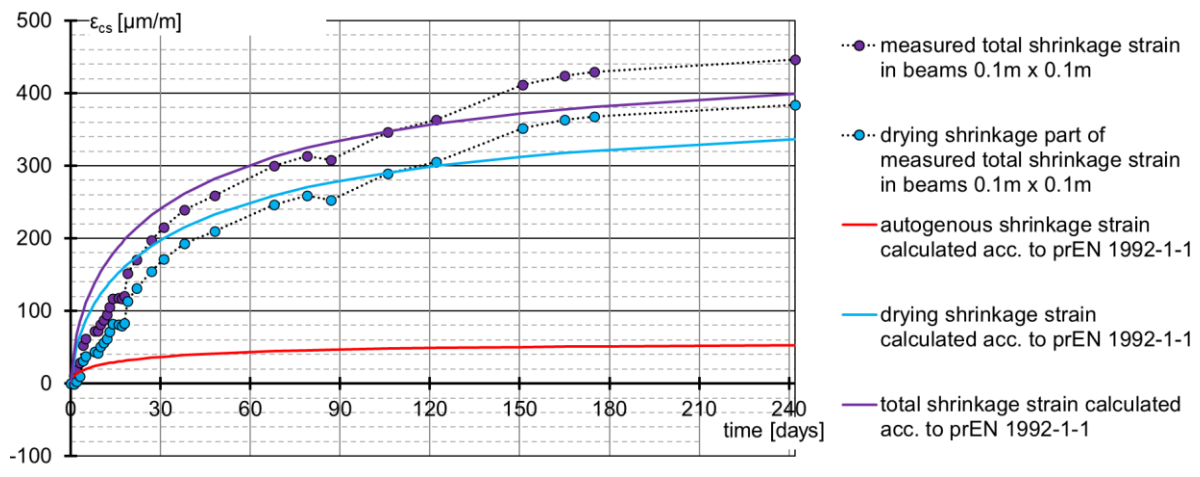


Figure A.11. Temperature measured along the height of the wall and its change in time

1109 The maximum hardening temperature of $\sim 48^{\circ}\text{C}$ was reached after approximately 24 hrs in the core of
1110 the wall (Fig. A.10). It is interesting to notice that the temperature at that moment was the highest at a
1111 relatively high level ($\sim 0.7H$) above the joint (Fig. A.11). Regarding the temperature difference in the
1112 cross-section, an important influence of diurnal temperature fluctuations and exposure was visible (Fig.
1113 A.10). Because of a relatively small thickness of the wall, at the time of the maximum temperature
1114 occurrence (Aug 26), the temperature difference between the core and the surface was at the level of up
1115 to $\sim 6^{\circ}\text{C}$ on the northern side of the wall, while on the southern, exposed side these differences reached
1116 even up to $\sim 15^{\circ}\text{C}$.

1117 After about 6 days the wall cooled down and its temperature was affected only by the ambient
1118 temperature, which oscillated around 20°C over the next 10 days (Fig. A.10). The temperature along
1119 the height of the wall in its core was almost uniform (Fig. A.11). In the long-term analysis of the
1120 temperature change it can be noticed that the wall was affected not only by the strains caused by the
1121 temperature drop but also temperature gradients in the cross-section. The differences between the core
1122 and surface temperature on the northern side did not exceed 3°C while on the southern side of the wall
1123 reached periodically even up to several degrees. It is interesting to notice the effect of exposure of the
1124 southern side – during the day the surface of the wall on this side was intensively heated by the sun
1125 which caused higher temperatures on the surface than in the core (Fig. A.10). Similar effect can be seen
1126 on the northern surface, but it is of much smaller magnitude. Over the period of the analysis the
1127 temperature of the wall decreased to almost 0°C (Fig. A.10), which means the temperature drop of
1128 almost 50°C .

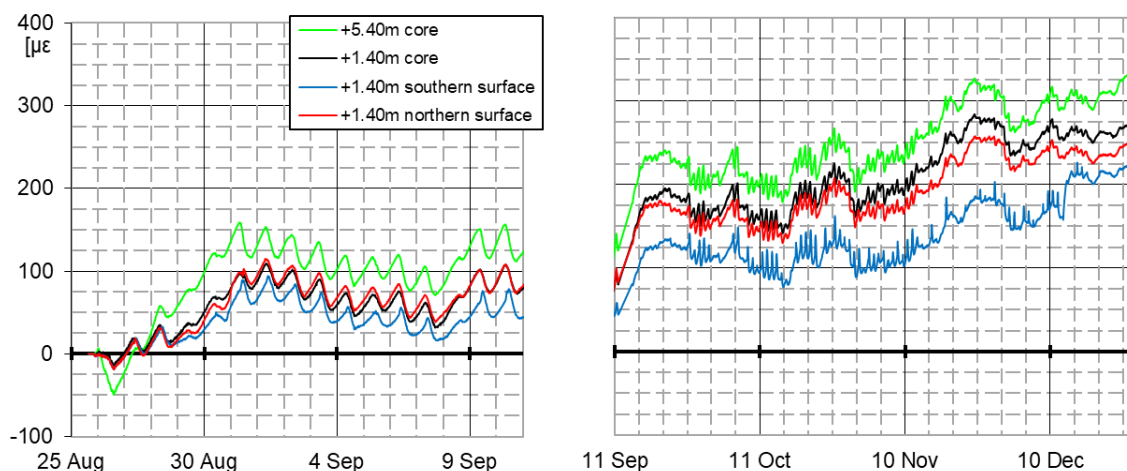
1129 Laboratory shrinkage strain measurements were performed on the concrete used for construction of the
1130 analysed tank wall segment. The tests were performed on the $10\text{ cm} \times 10\text{ cm}$ beams. Figure A.12
1131 presents the results of the measurements of the total strain for 8 months.



1132

1133 **Figure A.12.** Shrinkage strain of concrete used for construction of the tank wall measured in the laboratory
 1134 conditions and approximated with EN 1992-1-1:2023.

1135 Concrete strain measurements were also carried out on the wall with the use of embedment vibrating
 1136 wire sensors (for the arrangement see Fig. A.8). The first group of sensors was placed at the height of
 1137 +1.40 m. The second group of sensors was located in the upper part of the wall 1.3 m below the lower
 1138 edge of the crowning beam (at the level of + 5.40 m), which is the zone that usually does not crack, thus
 1139 allows to perform linear analysis. Figure A.13 presents the measurements of strains over the period of
 1140 first 4 months. This strain can be understood as a free part of the restrained strain. Therefore, it can be
 1141 observed that the biggest values of strains were recorded in the top part of the wall (at the level of +5.40
 1142 m) while the strains near the joint (at the level of + 1.40 m), where the level of restraint was lower, were
 1143 smaller. This was also the zone of the wall which cracked.



1144

1145

Figure A.13. Changes of measured strains in concrete over 4 months.

1146 The measured concrete strains were compared with the calculated strains. The total free strain was
1147 calculated as a sum of thermal strain, determined from the temperature change, and shrinkage strain,
1148 calculated based on the laboratory tests results. Calculations were performed in point where the B1
1149 sensor was located to compare the results with the measured strains. The thermal strain was calculated
1150 by multiplication of the temperature difference measured in the point B1, calculated in time steps of 15
1151 mins, by the coefficient of thermal expansion which value was taken as $10^{-5}/^{\circ}\text{C}$.
1152 Measurements of strains were sparser than the measurements of temperature. Therefore, it was
1153 necessary to define an approximation function to obtain intermediate results. The formulas proposed by
1154 EN 1992-1-1:2023 were used as they offer an improved prediction of shrinkage strains in comparison
1155 to EN 1992-1-1:2004. The approximation functions used in calculations are shown in Fig. A.12.

1156 The autogenous shrinkage development was approximated with a function:

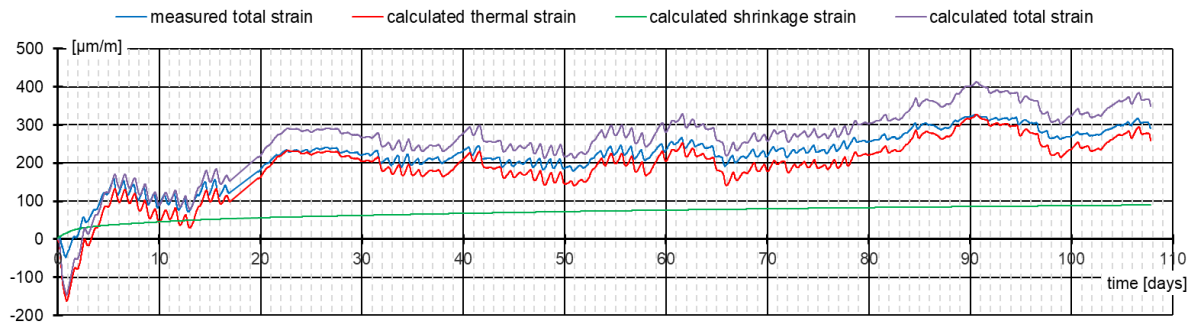
$$1157 \quad \beta_{ca}(t) = 1 - \exp(-0.2\sqrt{t}) \quad (\text{A.3})$$

1158 and the final value of the autogenous shrinkage determined for the applied class of concrete was $65 \mu\epsilon$.
1159 The autogenous shrinkage in the wall was calculated considering temperature dependence of the
1160 development rate using an equivalent age of concrete instead of the time based on the recorded
1161 temperature history. Autogenous shrinkage calculated with this approach was subtracted from the total
1162 measured shrinkage, and the result was treated as drying shrinkage part of the strain.

1163 The drying shrinkage development was approximated with the function:

$$1164 \quad \beta_{ca}(t) = \left[(t - t_s) / (t - t_s + 0.035h_0^2) \right]^{0.5} \quad (\text{A.4})$$

1165 with the final value of drying shrinkage equal to $393 \mu\epsilon$ and coefficient $\beta_{RH} = 1$. The predictions of the
1166 strain development in comparison to the measured strains are on a satisfactory level for the first 120
1167 days, so for the analysed period. The drying shrinkage in the wall was calculated using this formula for
1168 $t_s = 1 \text{ day}$, $h_0 = 600 \text{ mm}$.



1169

1170 **Figure A.14.** Comparison between the measured and calculated strain at the level of + 5.40 m in the tank wall.

1171 Figure A.14 shows comparison between the measured strain and the calculated strain in point B1, as

1172 well as the thermal strain and shrinkage strain in this location. It can be observed that the strain in the

1173 wall depends mostly on the thermal strain, which governs the behaviour of the strain change in time;

1174 thermal strain is also predicted to be about 4 times greater than the shrinkage strain. The calculated and

1175 measured strain in point B1 coincide quite well – significant difference is visible only at the stage of

1176 heating of the wall because the calculated strain does not take into account the effect of creep, which is

1177 known to be high in this period. The strains measured in point B1 can be treated as almost free strains

1178 and the free strain in the wall can be calculated with the above proposed approach.